

Computing the ground state and dynamics of the nonlinear Schrödinger equation with nonlocal interactions via the nonuniform FFT

Weizhu Bao

Department of Mathematics, National University of Singapore, Singapore
119076, Singapore

Shidong Jiang

Department of Mathematical Sciences, New Jersey Institute of Technology,
Newark, New Jersey, 07102, USA

Qinglin Tang

Université de Lorraine, Institut Elie Cartan de Lorraine, UMR 7502,
Vandoeuvre-lès-Nancy, F-54506, France

Inria Nancy Grand-Est/IECL-CORIDA, France

Yong Zhang

Wolfgang Pauli Institute c/o Fak. Mathematik, University Wien,
Oskar-Morgenstern-Platz 1, 1090 Vienna, Austria

Abstract

We present efficient and accurate numerical methods for computing the ground state and dynamics of the nonlinear Schrödinger equation (NLSE) with nonlocal interactions based on a fast and accurate evaluation of the long-range interactions via the nonuniform fast Fourier transform (NUFFT). We begin with a review of the fast and accurate method, proposed recently by two of the authors in [29], which evaluates the Coulomb interaction in three (3D) and two (2D) dimensions via the NUFFT. Then we extend the method to compute other nonlocal interactions which do not decay at far field, such as the interaction whose kernel is the Green's function of the Laplace operator in 2D and 1D. We compare numerically the performance of this method and other existing methods with particular attention on the effect of the size of the truncated bounded computational domain. For computing the ground state and dynamics, we propose efficient and accurate numerical methods based on the normalized gradient flow with backward Euler Fourier pseudospectral discretization and time-splitting Fourier pseudospectral method, respectively, together with the fast and accurate NUFFT method for evaluating the nonlocal interactions. Extensive numerical comparisons are carried out between these methods and other existing methods for computing the ground state and dynamics of the NLSE with nonlocal interactions. Numerical results show that the methods via the NUFFT perform much better than those existing methods in terms of accuracy and/or

efficiency for computing the ground state and dynamics as well as for evaluating the nonlocal interactions, especially when the bounded computational domain is chosen smaller.

1 Introduction

In this paper, we present efficient and accurate numerical methods and compare them with existing numerical methods for computing the ground state and dynamics of the nonlinear Schrödinger equation (NLSE), in dimensionless form, with a nonlocal (long-range) interaction in d -dimensions ($d = 3, 2, 1$) as

$$\begin{aligned} i \partial_t \psi(\mathbf{x}, t) &= \left[-\frac{1}{2} \Delta + V(\mathbf{x}) + \beta \varphi(\mathbf{x}, t) \right] \psi(\mathbf{x}, t), & \mathbf{x} \in \mathbb{R}^d, \quad t \geq 0; \\ \varphi(\mathbf{x}, t) &= (U * |\psi|^2)(\mathbf{x}, t), & \mathbf{x} \in \mathbb{R}^d, \quad t \geq 0; \end{aligned} \quad (1.2)$$

with the initial data

$$\psi(\mathbf{x}, t = 0) = \psi_0(\mathbf{x}), \quad \mathbf{x} \in \mathbb{R}^d. \quad (1.3)$$

Here, t is time, \mathbf{x} is the spatial coordinates, $\psi := \psi(\mathbf{x}, t)$ is the complex-valued wave-function, $V(\mathbf{x})$ is a given real-valued external potential, β is a dimensionless interaction constant (positive for repulsive interaction and negative for attractive interaction), and $\varphi := \varphi(\mathbf{x}, t)$ is a real-valued nonlocal (long-range) interaction which is defined as the convolution of an interaction kernel $U(\mathbf{x})$ and the density function $\rho := \rho(\mathbf{x}, t) = |\psi(\mathbf{x}, t)|^2$. The NLSE with the nonlocal interaction (1.1)-(1.2) has been widely used in modelling a variety of problems arising from quantum physics and chemistry to materials science and biology. It is nonlinear, dispersive and time transverse invariant, i.e. if $V(\mathbf{x}) \rightarrow V(\mathbf{x}) + \alpha$ and $\varphi(\mathbf{x}, t) \rightarrow \varphi(\mathbf{x}, t) + \delta$, then $\psi(\mathbf{x}, t) \rightarrow \psi(\mathbf{x}, t)e^{-i(\alpha+\delta)t}$, which immediately implies that the physical observables such as the density $\rho(\mathbf{x}, t) = |\psi(\mathbf{x}, t)|^2$ are unchanged. In addition, it conserves the *mass* and *energy* as

$$\begin{aligned} N(\psi(\cdot, t)) &:= \int_{\mathbb{R}^d} |\psi(\mathbf{x}, t)|^2 d\mathbf{x} \equiv \int_{\mathbb{R}^d} |\psi(\mathbf{x}, 0)|^2 d\mathbf{x} = \int_{\mathbb{R}^d} |\psi_0(\mathbf{x})|^2 d\mathbf{x} = N(\psi_0), & t \geq 0; \\ E(\psi(\cdot, t)) &:= \int_{\mathbb{R}^d} \left[\frac{1}{2} |\nabla \psi(\mathbf{x}, t)|^2 + V(\mathbf{x}) |\psi(\mathbf{x}, t)|^2 + \frac{1}{2} \beta \varphi(\mathbf{x}, t) |\psi(\mathbf{x}, t)|^2 \right] d\mathbf{x} \equiv E(\psi_0). \end{aligned} \quad (1.4)$$

One of the most important nonlocal interactions in applications is the

Coulomb interaction whose interaction kernel in 3D/2D is given as

$$U_{\text{Cou}}(\mathbf{x}) = \begin{cases} \frac{1}{4\pi|\mathbf{x}|}, \\ \frac{1}{2\pi|\mathbf{x}|}, \end{cases} \quad \iff \quad \widehat{U}_{\text{Cou}}(\boldsymbol{\xi}) = \begin{cases} \frac{1}{|\mathbf{k}|^2}, & d = 3, \\ \frac{1}{|\mathbf{k}|}, & d = 2, \end{cases} \quad \mathbf{x}, \mathbf{k} \in \mathbb{R}^d, \quad (1.6)$$

where $\widehat{f}(\mathbf{k}) = \int_{\mathbb{R}^d} f(\mathbf{x}) e^{-i\mathbf{k}\cdot\mathbf{x}} d\mathbf{x}$ is the Fourier transform of $f(\mathbf{x})$ for $\mathbf{x}, \mathbf{k} \in \mathbb{R}^d$. In 3D, the Coulomb interaction kernel $U_{\text{Cou}}(\mathbf{x})$ is exactly the Green's function of the Laplace operator and thus the nonlocal Coulomb interaction φ in (1.2) also satisfies the Poisson equation in 3D

$$-\Delta \varphi(\mathbf{x}, t) = |\psi(\mathbf{x}, t)|^2, \quad \mathbf{x} \in \mathbb{R}^3, \quad \lim_{|\mathbf{x}| \rightarrow \infty} \varphi(\mathbf{x}, t) = 0, \quad t \geq 0. \quad (1.7)$$

In this case, (1.1)-(1.2) is also referred as the 3D Schrödinger-Poisson system (SPS) which was derived from the linear Schrödinger equation for a many-body (e.g. N electrons) quantum system with binary Coulomb interaction between different electrons via the ‘‘mean field limit’’ [12, 13, 14, 23]. It has important applications in modelling semiconductor devices and calculating electronic structures in materials simulation and design. On the other hand, the Coulomb interaction kernel $U(\mathbf{x})$ in 2D is the Green's function of the square-root-Laplace operator instead of the Laplace operator and thus the nonlocal Coulomb interaction φ in (1.2) also satisfies the fractional Poisson equation in 2D

$$\sqrt{-\Delta} \varphi(\mathbf{x}, t) = |\psi(\mathbf{x}, t)|^2, \quad \mathbf{x} \in \mathbb{R}^2, \quad \lim_{|\mathbf{x}| \rightarrow \infty} \varphi(\mathbf{x}, t) = 0, \quad t \geq 0 \quad (1.8)$$

In this case, (1.1)-(1.2) could be obtained from the 3D SPS under an infinitely strong external confinement in the z -direction [9, 15]. This model could be used for modelling 2D materials such as graphene and ‘‘electron sheets’’ [20].

Another type of interaction from applications is that the interaction kernel $U(\mathbf{x})$ is taken as the Green's function of the Laplace operator in 3D/2D/1D [41]

$$U_{\text{Lap}}(\mathbf{x}) = \begin{cases} \frac{1}{4\pi|\mathbf{x}|}, & d = 3, \\ -\frac{1}{2\pi} \ln |\mathbf{x}|, & d = 2, \\ -\frac{1}{2} |\mathbf{x}|, & d = 1, \end{cases} \quad \iff \quad \widehat{U}_{\text{Lap}}(\mathbf{k}) = \frac{1}{|\mathbf{k}|^2}, \quad \mathbf{x}, \mathbf{k} \in \mathbb{R}^d.$$

(1.9)

When $d = 3$, $U_{\text{Lap}}(\mathbf{x}) = U_{\text{Cou}}(\mathbf{x})$ for $\mathbf{x} \in \mathbb{R}^3$. When $d = 2$, the nonlocal interaction φ in (1.2) with (1.9), which is called the Poisson potential for simplicity, also satisfies the Poisson equation in 2D with the given far-field condition

$$-\Delta \varphi(\mathbf{x}, t) = |\psi(\mathbf{x}, t)|^2, \quad \mathbf{x} \in \mathbb{R}^2, \quad \lim_{|\mathbf{x}| \rightarrow \infty} \left[\varphi(\mathbf{x}, t) + \frac{C_0}{2\pi} \ln |\mathbf{x}| \right] = 0, \quad t \geq 0; \quad (1.10)$$

and when $d = 1$ with $\mathbf{x} = x$, it satisfies the Poisson equation in 1D with the given far-field condition

$$-\partial_{xx} \varphi(x, t) = |\psi(x, t)|^2, \quad x \in \mathbb{R}, \quad \lim_{x \rightarrow \pm\infty} \left[\varphi(x, t) + \frac{1}{2} (C_0|x| \mp C_1) \right] = 0, \quad t \geq 0, \quad (1.11)$$

where $C_0 = \int_{\mathbb{R}^d} |\psi(\mathbf{x}, t)|^2 d\mathbf{x} = \widehat{|\psi|^2}(\mathbf{0}, t) \equiv \int_{\mathbb{R}^d} |\psi_0(\mathbf{x})|^2 d\mathbf{x} = \widehat{|\psi_0|^2}(\mathbf{0}) = N(\psi_0)$ and $C_1 = \int_{\mathbb{R}} x |\psi(x, t)|^2 dx = \widehat{(x|\psi|^2)}(\mathbf{0}, t)$, which indicate that the nonlocal interaction $\varphi(\mathbf{x}, t) \rightarrow -\infty$ as $|\mathbf{x}| \rightarrow \infty$ in 2D/1D. In fact, when $d = 2$ and/or $d = 1$, (1.1)-(1.2) with (1.9) is also referred as the 2D and/or 1D SPS. They could be obtained from the 3D SPS by integrating the 3D Coulomb interaction kernel $U_{\text{Cou}}(\mathbf{x})$ along the z -line and/or (y, z) -plane under the assumption that the electrons are uniformly distributed in one and/or two spatial dimensions, respectively. The 2D/1D SPS is usually used for modelling 2D “electron sheets” and 1D “quantum wires”, respectively, as well as lower dimensions semiconductor devices [32].

Recently, the following nonlocal interaction kernels in 2D/1D were obtained from the 3D SPS under strongly confining external potentials in the z -direction and (y, z) -plane, respectively

$$U_{\text{Con}}^\varepsilon(\mathbf{x}) = \begin{cases} \frac{2}{(2\pi)^{3/2}} \int_0^\infty \frac{e^{-\frac{u^2}{2}}}{\sqrt{|\mathbf{x}|^2 + \varepsilon^2 u^2}} du, & \mathbf{x} \in \mathbb{R}^2 \\ \frac{1}{4} \int_0^\infty \frac{e^{-\frac{u^2}{2}}}{\sqrt{|\mathbf{x}|^2 + \varepsilon^2 u}} du, & \mathbf{x} \in \mathbb{R} \end{cases} \iff \widehat{U}_{\text{Con}}^\varepsilon(\mathbf{k}) = \begin{cases} \frac{2}{\pi} \int_0^\infty \frac{e^{-\frac{\varepsilon^2 s^2}{2}}}{|\mathbf{k}|^2 + s^2} ds, & \mathbf{k} \in \mathbb{R}^2, \\ \frac{1}{2} \int_0^\infty \frac{e^{-\varepsilon^2 s/2}}{|\mathbf{k}|^2 + s} ds, & \mathbf{k} \in \mathbb{R}, \end{cases} \quad (1.12)$$

where $0 < \varepsilon \ll 1$ is a dimensionless constant describing the ratio of the anisotropic confinement in different directions in the original 3D SPS [9].

In this case, the convolution (1.2) for the nonlocal interaction φ can no longer be re-formulated into a partial differential equation. For other nonlocal interactions considered in quantum chemistry and dipole Bose-Einstein condensation, e.g. the dipole-dipole interaction, we refer to [4, 5, 17, 29] and references therein.

The ground state of the NLSE is defined as follows: find $\phi_g(\mathbf{x}) \in S$ such that

$$E(\phi_g) = \min_{\phi \in S} E(\phi), \quad \text{with} \quad S := \{\phi(\mathbf{x}) \mid \|\phi\|^2 := \int_{\mathbb{R}^d} |\phi(\mathbf{x})|^2 d\mathbf{x} = 1, E(\phi) < \infty\}. \quad (1.13)$$

For the existence, uniqueness and exponentially decay properties of the ground state ϕ_g as well as the well-posedness and dynamical properties of the NLSE, we refer to [36, 18, 16, 4, 15, 19, 33, 34] and references therein.

In order to numerically compute the ground state of (1.13) and the dynamics of (1.1)-(1.2), one of the key difficulties is how to efficiently and accurately evaluate the nonlocal interaction (1.2) with a given density $\rho = |\psi|^2$. As we know, for a convolution, the most efficient and natural way is to use the Fourier transform, i.e. to re-formulate (1.2) as

$$\varphi(\mathbf{x}, t) = \frac{1}{(2\pi)^d} \int_{\mathbb{R}^d} \widehat{U}(\mathbf{k}) \widehat{|\psi|^2}(\mathbf{k}, t) e^{i\mathbf{k}\cdot\mathbf{x}} d\mathbf{k} = \frac{1}{(2\pi)^d} \int_{\mathbb{R}^d} \widehat{U}(\mathbf{k}) \widehat{\rho}(\mathbf{k}, t) e^{i\mathbf{k}\cdot\mathbf{x}} d\mathbf{k}, \quad \mathbf{x} \in \mathbb{R}^d, \quad t \geq 0. \quad (1.14)$$

Then the integral on the right hand side will be truncated on a bounded computational domain $\Omega \subset \mathbb{R}^d$ and be evaluated via fast Fourier transform (FFT) [11]. However, this approach is hampered by the fact that the Fourier transform of the interaction kernel $\widehat{U}(\mathbf{k})$ has a singularity and/or $\widehat{\rho}(\mathbf{k}, t) = \widehat{|\psi|^2}(\mathbf{k}, t) \neq 0$ at the origin $\mathbf{k} = \mathbf{0}$ in Fourier (phase) space. In fact, for the Coulomb interaction in 3D, it is the equivalent of first truncating the Poisson equation (1.7) on a bounded computational domain Ω , e.g. a box, with periodic boundary condition on $\partial\Omega$, and then discretizing the truncated problem by the Fourier spectral method. It is easy to see that this approach introduces a numerical paradox due to the improper periodic boundary conditions on $\partial\Omega$ as follows:

$$0 < \int_{\Omega} |\psi(\mathbf{x}, t)|^2 d\mathbf{x} = - \int_{\Omega} \Delta\varphi(\mathbf{x}, t) d\mathbf{x} = - \int_{\partial\Omega} \frac{\partial\varphi}{\partial\mathbf{n}} ds = 0. \quad (1.15)$$

Thus, this approach suffers from no convergence in terms of the mesh size of partitioning Ω when it is small for a given Ω (a phenomenon known as

“numerical locking” in the literature) and its convergence is very slow, e.g. linearly convergent for the 3D/2D Coulomb interaction, in terms of the size of Ω because φ decays only linearly although ψ decays exponentially when $|\mathbf{x}| \rightarrow \infty$. To overcome the numerical paradox (1.15) in using FFT for evaluating the nonlocal interaction (1.2), for the Coulomb interaction (1.6) in 3D/2D, due to the fact that the nonlocal interaction potential $\varphi(\mathbf{x}, t)$ decays to zero at far field, a numerical method was proposed by truncating (1.7) in 3D and (1.8) in 2D on a bounded computational domain Ω , e.g. a box in 3D and a rectangle in 2D, with homogeneous Dirichlet boundary condition on $\partial\Omega$, and then to discretize the truncated problem by the spectral method with sine basis via discrete sine transform (DST) [6, 17, 41]. This method avoids numerically the singularity of $\hat{U}(\mathbf{k})$ at the origin $\mathbf{k} = \mathbf{0}$ and thus significantly improves the accuracy in the evaluation of the Coulomb interaction potential. Because the Coulomb interaction potential φ decays only linearly when $|\mathbf{x}| \rightarrow \infty$, the truncation error in this method decays only linearly in terms of the size of the bounded computational domain Ω . Thus when high accuracy is required, the bounded computational domain Ω must be chosen very large, which causes significantly numerical burden in memory and computational cost for evaluating the nonlocal interaction potential (1.2) and/or solving the NLSE (1.1). In fact, in most applications, the wavefunction ψ decays exponentially when $|\mathbf{x}| \rightarrow \infty$, therefore the NLSE (1.1) could be truncated on a much smaller bounded computational domain! Of course, this method could not be extended to the case where $U(\mathbf{x})$ in (1.1) is taken as either (1.9) or (1.12).

Very recently, a fast and accurate algorithm was proposed for the evaluation of the nonlocal interaction (1.2) with the Coulomb interaction kernel (1.6) in 3D/2D via the nonuniform FFT (NUFFT) [29]. The key idea in the algorithm is to re-formulate the integral on the right hand side of (1.14) via spherical and polar coordinates in phase space in 3D and 2D, respectively, then the singularity in $\hat{U}(\mathbf{k})$ at the origin is canceled and thus the integrand becomes a smooth function. Then the integral can be approximated via a high-order discretization of the Fourier integral, accelerated by NUFFT [29]. The algorithm was demonstrated numerically to be efficient, e.g. at $O(N \log N)$ complexity with N the total number of unknowns, and can achieve very high accuracy for the evaluation of the Coulomb interaction [29]. The main aims of this paper are fourfold: (i) to extend the fast and accurate algorithm based on the NUFFT for the evaluation of the Coulomb interaction to the general nonlocal interaction (1.2) including the case where $U(\mathbf{x})$ is taken as (1.9) and the singularity in $\hat{U}_{\text{Lap}}(\mathbf{k})$ at the origin cannot be canceled via using the polar coordinates in the phase space in 2D; (ii) to com-

pare numerically the method based on the NUFFT with existing numerical methods that are based on FFT or DST for the evaluation of the nonlocal interaction in terms of the size of the bounded computational domain Ω and the mesh size of partitioning Ω ; (iii) to propose efficient and accurate numerical methods for computing the ground state and dynamics of the NLSE with the nonlocal interaction (1.1)-(1.2) by coupling the algorithm based on the NUFFT for the evaluation of the nonlocal interaction with the normalized gradient flow with backward Euler Fourier pseudospectral discretization and time-splitting Fourier pseudospectral method, respectively, and (iv) to compare these methods numerically with those existing numerical methods based on FFT or DST for computing the ground state and dynamics of the NLSE by paying particular attention on the effect of the mesh size and the size of the bounded computational domain Ω .

This paper is organized as follows. In Section 2, we briefly review the fast and accurate algorithm based on the NUFFT in [29] for the evaluation of the Coulomb interaction in 3D/2D, and then extend it to the general nonlocal interaction (1.2) including the case where $U(\mathbf{x})$ is taken as either (1.9) or (1.12). In Section 3, we present an efficient and accurate numerical method for computing the ground state of the NLSE (1.1)-(1.2) by coupling the efficient and accurate evaluation of the nonlocal interaction via the NUFFT and the normalized gradient flow discretized with the backward Euler Fourier pseudospectral method, and compare the performance of this method and those existing numerical methods. Similarly in Section 4, an efficient and accurate numerical method is proposed for computing the dynamics of the NLSE by coupling the efficient and accurate evaluation of the nonlocal interaction via the NUFFT and the time-splitting Fourier pseudospectral method. Finally, some concluding remarks are drawn in Section 5.

2 An algorithm for the evaluation of the nonlocal interaction via the NUFFT

In this section, we will propose a fast and accurate evaluation of the nonlocal interaction

$$u(\mathbf{x}) = (U * \rho)(\mathbf{x}) = \frac{1}{(2\pi)^d} \int_{\mathbb{R}^d} \widehat{U}(\mathbf{k}) \widehat{\rho}(\mathbf{k}) e^{i\mathbf{k} \cdot \mathbf{x}} d\mathbf{k}, \quad \mathbf{x} \in \mathbb{R}^d, \quad d = 3, 2, 1, \quad (2.1)$$

where $\rho := \rho(\mathbf{x}) \geq 0$ for $\mathbf{x} \in \mathbb{R}^d$ is a given smooth density function rapidly decaying at far field and satisfies $C_0 := \widehat{\rho}(\mathbf{0}) = \int_{\mathbb{R}^d} \rho(\mathbf{x}) d\mathbf{x} > 0$. We will first briefly review the algorithm via the NUFFT which was proposed recently in [29] for fast and accurate evaluation of the Coulomb interactions in 3D and 2D, and then extend the algorithm to the cases where $U(\mathbf{x})$ in (2.1) is taken as either (1.9) or (1.12).

2.1 For the Coulomb interactions in 3D/2D

When $U(\mathbf{x})$ in (2.1) is taken as the the Coulomb interaction kernel (1.6), by truncating the integration domain in (2.1) into a bounded domain and adopting the spherical/polar coordinates in 3D/2D, respectively, in the Fourier (or phase) space, we have [29]

$$\begin{aligned} u(\mathbf{x}) &= \frac{1}{(2\pi)^d} \int_{\mathbb{R}^d} e^{i\mathbf{k}\cdot\mathbf{x}} \widehat{U}_{\text{Cou}}(\mathbf{k}) \widehat{\rho}(\mathbf{k}) d\mathbf{k} = \frac{1}{(2\pi)^d} \int_{\mathbb{R}^d} \frac{1}{|\mathbf{k}|^{d-1}} e^{i\mathbf{k}\cdot\mathbf{x}} \widehat{\rho}(\mathbf{k}) d\mathbf{k} \\ &\approx \frac{1}{(2\pi)^d} \int_{|\mathbf{k}| \leq P} \frac{1}{|\mathbf{k}|^{d-1}} e^{i\mathbf{k}\cdot\mathbf{x}} \widehat{\rho}(\mathbf{k}) d\mathbf{k} \\ &= \frac{1}{(2\pi)^d} \begin{cases} \int_0^P \int_0^\pi \int_0^{2\pi} e^{i\mathbf{k}\cdot\mathbf{x}} \widehat{\rho}(\mathbf{k}) \sin \theta d|k| d\theta d\phi, & d = 3, \\ \int_0^P \int_0^{2\pi} e^{i\mathbf{k}\cdot\mathbf{x}} \widehat{\rho}(\mathbf{k}) d|k| d\phi, & d = 2, \end{cases} \quad \mathbf{x} \in \Omega \subset (\mathbb{R}^d) \end{aligned}$$

Here, $P = O(1/\varepsilon_0)^{1/n}$, $\varepsilon_0 > 0$ is the prescribed precision, e.g. $\varepsilon_0 = 10^{-10}$, and the positive integer n , the regularity of the density, is the decaying rate of $\widehat{\rho}(\mathbf{k})$ at far field, i.e. $\widehat{\rho}(\mathbf{k}) = O(|\mathbf{k}|^{-n})$ as $|\mathbf{k}| \rightarrow \infty$. Correspondingly, we choose a bounded domain Ω large enough such that the truncation error of $\rho(\mathbf{x})$ is negligible. It is easy to see that the singularities at the origin in phase space has been removed by a coordinate transformation to spherical and polar coordinates in 3D and 2D, respectively. Thus, the above integral can be discretized using high order quadratures and the resulting summation can be evaluated efficiently with the help of the NUFFT. This leads to an $O(N \log N) + O(M)$ algorithm where N is the total number of equispaced points in the physical space and M is the number of nonequispaced points for partitioning $B = \{\mathbf{k} \in \mathbb{R}^d \mid |\mathbf{k}| \leq P\}$ in the Fourier space. However, M is roughly N and the constant in front of $O(M)$ is much greater than the constant in front of $O(N \log N)$, which makes the algorithm slower than the regular FFT by a large factor, especially for three dimensional problems.

In order to reduce the computational cost in the NUFFT, the integral

in (2.2) is further split into two parts by using a simple partition of unity:

$$\begin{aligned}
u(\mathbf{x}) &\approx \frac{1}{(2\pi)^d} \int_{|\mathbf{k}| \leq P} \frac{1}{|\mathbf{k}|^{d-1}} e^{i\mathbf{k} \cdot \mathbf{x}} \widehat{\rho}(\mathbf{k}) d\mathbf{k} \\
&= \frac{1}{(2\pi)^d} \int_{|\mathbf{k}| \leq P} e^{i\mathbf{k} \cdot \mathbf{x}} \frac{1 - p_d(\mathbf{k})}{|\mathbf{k}|^{d-1}} \widehat{\rho}(\mathbf{k}) d\mathbf{k} + \frac{1}{(2\pi)^d} \int_{|\mathbf{k}| \leq P} e^{i\mathbf{k} \cdot \mathbf{x}} \frac{p_d(\mathbf{k})}{|\mathbf{k}|^{d-1}} \widehat{\rho}(\mathbf{k}) d\mathbf{k} \\
&\approx \frac{1}{(2\pi)^d} \int_{\mathcal{D}} e^{i\mathbf{k} \cdot \mathbf{x}} w_d(\mathbf{k}) \widehat{\rho}(\mathbf{k}) d\mathbf{k} + \frac{1}{(2\pi)^d} \int_{|\mathbf{k}| \leq P} e^{i\mathbf{k} \cdot \mathbf{x}} \frac{p_d(\mathbf{k})}{|\mathbf{k}|^{d-1}} \widehat{\rho}(\mathbf{k}) d\mathbf{k} := I_1 + I_2, \quad \mathbf{x} \in \Omega
\end{aligned}$$

Here, $\mathcal{D} = \{\mathbf{k} = (k_1, \dots, k_d)^T \mid -P \leq k_j \leq P, j = 1, \dots, d\}$ is a rectangular domain containing the ball B , the function $p_d(\mathbf{k})$ is chosen such that it is a C^∞ function that decays exponentially fast as $|\mathbf{k}| \rightarrow \infty$ and the function $w_d(\mathbf{k}) := \frac{1 - p_d(\mathbf{k})}{|\mathbf{k}|^{d-1}}$ is smooth for $\mathbf{k} \in \mathbb{R}^d$. With this $p_d(\mathbf{k})$, I_1 can be computed via the regular FFT and I_2 can be evaluated via the NUFFT with a fixed number of irregular points in the Fourier space. Thus the interpolation cost in the NUFFT is reduced to $O(1)$ and the cost of the overall algorithm is comparable to that of the regular FFT, with an oversampling factor (2^3 for 3D problems and $2^2 - 3^2$ for 2D problems) in front of $O(N \log N)$. In many applications, the function $p_d(\mathbf{k})$ can be chosen as a Gaussian, e.g. $p_d(\mathbf{k}) = e^{-|\mathbf{k}|^2/a}$, $a > 0$ is a positive parameter. In this case, $w_3(\mathbf{0}) = \frac{1}{a}$ when $d = 3$ and $w_2(\mathbf{0}) = 0$ when $d = 2$. For more details, we refer to [29] and references therein.

2.2 For the Poisson potentials in 2D/1D

When $U(\mathbf{x})$ in (2.1) is taken as the the Green's function of the Laplace operator $U_{\text{Lap}}(\mathbf{x})$ (1.9) in 2D/1D, unfortunately, the algorithm based on the NUFFT discussed in the previous section cannot be applied directly to evaluate the Poisson potential $u(\mathbf{x})$ due to the stronger singularity of $\widehat{U}_{\text{Lap}}(\mathbf{k}) = \frac{1}{|\mathbf{k}|^2}$ at the origin $\mathbf{k} = \mathbf{0}$. Moreover, noticing (1.9) and (1.10), (2.1) can be re-formulated as the following Poisson equation with the proper far-field condition in 2D as

$$-\Delta u(\mathbf{x}) = |\rho(\mathbf{x})|^2, \quad \mathbf{x} \in \mathbb{R}^2, \quad \lim_{|\mathbf{x}| \rightarrow \infty} \left[u(\mathbf{x}) + \frac{\widehat{\rho}(\mathbf{0})}{2\pi} \ln |\mathbf{x}| \right] = 0, \quad (2.4)$$

and in 1D as (we denote \mathbf{x} as x and \mathbf{k} as k for scalar variables for simplicity)

$$-u''(x) = |\rho(x)|^2, \quad x \in \mathbb{R}, \quad \lim_{x \rightarrow \pm\infty} \left[u(x) + \frac{1}{2} \left(\widehat{\rho}(0)|x| \mp (\widehat{x\rho})(0) \right) \right] = 0, \quad (2.5)$$

which immediately implies that $u(\mathbf{x}) \rightarrow -\infty$ as $|\mathbf{x}| \rightarrow \infty$. Hence, (2.4) and (2.5) cannot be truncated into a bounded domain with the periodic, homogeneous Dirichlet or Neumann BC.

Let us first consider the 2D Poisson potential. To overcome the above mentioned difficulties, we introduce the auxiliary functions

$$G(\mathbf{x}) = \frac{1}{2\pi\sigma^2} e^{-\frac{|\mathbf{x}|^2}{2\sigma^2}}, \quad G_1(\mathbf{x}) = \widehat{\rho}(\mathbf{0}) G(\mathbf{x}) - \widehat{(\mathbf{x}\rho)}(\mathbf{0}) \cdot \nabla_{\mathbf{x}} G(\mathbf{x}), \quad \mathbf{x} \in \mathbb{R}^2, \quad (2.6)$$

and the function $u_1(\mathbf{x})$ which satisfies the Poisson equation with the far-field condition:

$$-\Delta u_1(\mathbf{x}) = G_1(\mathbf{x}), \quad \mathbf{x} \in \mathbb{R}^2, \quad \lim_{|\mathbf{x}| \rightarrow \infty} \left[u_1(\mathbf{x}) + \frac{\widehat{\rho}(\mathbf{0})}{2\pi} \ln |\mathbf{x}| \right] = 0. \quad (2.7)$$

Here, $\sigma > 0$ is a parameter to be chosen later. Solving (2.7) via the convolution, we have

$$u_1(\mathbf{x}) = (U_{\text{Lap}} * G_1)(\mathbf{x}) = \widehat{\rho}(\mathbf{0}) u_{1,1}(\mathbf{x}) - \widehat{(\mathbf{x}\rho)}(\mathbf{0}) \cdot \mathbf{u}_{1,2}(\mathbf{x}), \quad \mathbf{x} \in \mathbb{R}^2, \quad (2.8)$$

where

$$u_{1,1}(\mathbf{x}) = (U_{\text{Lap}} * G)(\mathbf{x}), \quad \mathbf{u}_{1,2}(\mathbf{x}) = \nabla_{\mathbf{x}} u_{1,1}(\mathbf{x}), \quad \mathbf{x} \in \mathbb{R}^2. \quad (2.9)$$

Note that $G(\mathbf{x})$ is radially symmetric, i.e. $G(\mathbf{x}) = G(|\mathbf{x}|) = G(r)$ with $r = |\mathbf{x}| \geq 0$ and $u_{1,1}(\mathbf{x})$ satisfies the Poisson equation

$$-\Delta u_{1,1}(\mathbf{x}) = G(\mathbf{x}), \quad \mathbf{x} \in \mathbb{R}^2, \quad \lim_{|\mathbf{x}| \rightarrow \infty} \left[u_{1,1}(\mathbf{x}) + \frac{1}{2\pi} \ln |\mathbf{x}| \right] = 0, \quad (2.10)$$

we can easily conclude that $u_{1,1}(\mathbf{x})$ is also radially symmetric, i.e. $u_{1,1}(\mathbf{x}) = u_{1,1}(r)$. Thus, the Poisson equation (2.10) can be re-formulated as the following second order ODE:

$$-\frac{1}{r} \partial_r (r \partial_r u_{1,1}(r)) = G(r), \quad 0 < r < \infty, \quad \lim_{r \rightarrow \infty} \left[u_{1,1}(r) + \frac{1}{2\pi} \ln r \right] = 0. \quad (2.11)$$

Integrating the above ODE twice with respect to r and noticing the boundary conditions, we obtain

$$u_{1,1}(\mathbf{x}) = \begin{cases} -\frac{1}{4\pi} \left[\mathbb{E}_1\left(\frac{|\mathbf{x}|^2}{2\sigma^2}\right) + 2 \ln(|\mathbf{x}|) \right], & \mathbf{x} \neq \mathbf{0}, \\ \frac{1}{4\pi} (\gamma_e - \ln(2\sigma^2)), & \mathbf{x} = \mathbf{0}, \end{cases} \quad \mathbf{x} \in \mathbb{R}^2, \quad (2.12)$$

where $\mathbb{E}_1(r) := \int_r^\infty t^{-1} e^{-t} dt$ for $r > 0$ is the exponential integral function [1] and $\gamma_e \approx 0.5772156649015328606$ is the Euler-Mascheroni constant. Inserting (2.12) into (2.9), we get

$$\mathbf{u}_{1,2}(\mathbf{x}) = \begin{cases} -\frac{1}{2\pi} \frac{\mathbf{x}}{|\mathbf{x}|^2} \left(1 - e^{-\frac{|\mathbf{x}|^2}{2\sigma^2}} \right), & \mathbf{x} \neq \mathbf{0}, \\ 0, & \mathbf{x} = \mathbf{0}, \end{cases} \quad \mathbf{x} \in \mathbb{R}^2. \quad (2.13)$$

Denote

$$u_2(\mathbf{x}) = u(\mathbf{x}) - u_1(\mathbf{x}) \quad \iff \quad u(\mathbf{x}) = u_1(\mathbf{x}) + u_2(\mathbf{x}), \quad \mathbf{x} \in \mathbb{R}^2, \quad (2.14)$$

and then subtract (2.14) from (2.4), we have

$$-\Delta u_2(\mathbf{x}) = \rho(\mathbf{x}) - G_1(\mathbf{x}), \quad \mathbf{x} \in \mathbb{R}^2, \quad \lim_{|\mathbf{x}| \rightarrow \infty} u_2(\mathbf{x}) = 0. \quad (2.15)$$

Solving the above problem via the Fourier integral, noticing (2.6) and using the fact that

$$\nabla_{\mathbf{k}} \widehat{\rho}(\mathbf{0}) = -i (\widehat{\mathbf{x}\rho})(\mathbf{0}) = -i \int_{\mathbb{R}^2} \mathbf{x} \rho(\mathbf{x}) d\mathbf{x},$$

we obtain

$$\begin{aligned} u_2(\mathbf{x}) &= (U_{\text{Lap}} * (\rho - G_1))(\mathbf{x}) = \frac{1}{(2\pi)^2} \int_{\mathbb{R}^2} \frac{\widehat{\rho}(\mathbf{k}) - \widehat{G}_1(\mathbf{k})}{|\mathbf{k}|^2} e^{i\mathbf{k}\cdot\mathbf{x}} d\mathbf{k} \\ &= \frac{1}{(2\pi)^2} \int_{\mathbb{R}^2} \frac{W(\mathbf{k})}{|\mathbf{k}|} e^{i\mathbf{k}\cdot\mathbf{x}} d\mathbf{k} \approx \frac{1}{(2\pi)^2} \int_0^P \int_0^{2\pi} W(\mathbf{k}) e^{i\mathbf{k}\cdot\mathbf{x}} d|\mathbf{k}| d\theta, \quad \mathbf{x} \in \Omega \subset \mathbb{R}^2, \end{aligned}$$

where

$$W(\mathbf{k}) = \begin{cases} \frac{\widehat{\rho}(\mathbf{k}) - \widehat{G}_1(\mathbf{k})}{|\mathbf{k}|} = \frac{\widehat{\rho}(\mathbf{k}) - (\widehat{\rho}(\mathbf{0}) + \mathbf{k} \cdot \nabla_{\mathbf{k}} \widehat{\rho}(\mathbf{0})) e^{-\frac{1}{2}|\mathbf{k}|^2 \sigma^2}}{|\mathbf{k}|}, & \mathbf{k} \neq \mathbf{0}, \\ 0, & \mathbf{k} = \mathbf{0}, \end{cases} \quad \mathbf{k} \in \mathbb{R}^2. \quad (2.17)$$

Now that the singularity of $W(\mathbf{k})/|\mathbf{k}|$ at the origin $\mathbf{k} = \mathbf{0}$ in (2.16) can be removed by switching to polar coordinates in the Fourier space, $u_2(\mathbf{x})$ can be evaluated by the fast and accurate algorithm via NUFFT discussed in the previous subsection and the details are omitted here for brevity.

In practical computations, the parameter σ in (2.6) should be chosen appropriately such that the Gaussian $e^{-\frac{1}{2}|\mathbf{k}|^2\sigma^2}$ and $\mathbf{k} \cdot \nabla_{\mathbf{k}}\widehat{\rho}(\mathbf{0})e^{-\frac{1}{2}|\mathbf{k}|^2\sigma^2}$ in the Fourier space decay at the same rate or faster than $\widehat{\rho}(\mathbf{k})$ when $|\mathbf{k}|$ is large. With this choice of σ , there is no need to enlarge the computational domain in the Fourier space for the evaluation of (2.16) via the NUFFT. On the other hand, there is no need to oversample the truncated Fourier domain due to the rapid decaying of the Gaussian $e^{-\frac{1}{2}|\mathbf{k}|^2\sigma^2}$ in the Fourier space. Thus, setting the Gaussian to $2 \cdot 10^{-16}$ at $|\mathbf{k}|_{\infty} = P$ with P being the side-length of the bounded computational box $B = \{\mathbf{k} \mid |\mathbf{k}| \leq P\}$ in the Fourier space, we can choose $\sigma = 6/P$, a constant that is independent of the density function ρ .

For the convenience of the readers, we summarize the algorithm to evaluate the Poisson potential $u(\mathbf{x})$ in 2D in Algorithm 1:

Algorithm 1 Evaluation of the Poisson potential in 2D

- Compute $\widehat{\rho}(\mathbf{k})$ and $\widehat{(\mathbf{x}\rho)}(\mathbf{0})$.
 - Evaluate $u_1(\mathbf{x}) = u_{1,1}(\mathbf{x}) + u_{1,2}(\mathbf{x})$ via (2.12) and (2.13).
 - Evaluate $u_2(\mathbf{x})$ through (2.16) via the NUFFT [29].
 - Compute $u(\mathbf{x}) = u_1(\mathbf{x}) + u_2(\mathbf{x})$.
-

Similarly, for the 1D case, i.e. $U_{\text{Lap}}(x) = -\frac{1}{2}|x|$, we introduce the auxiliary functions

$$G(x) = \frac{1}{\sqrt{2\pi}\sigma} e^{-\frac{x^2}{2\sigma^2}}, \quad G_1(x) = \widehat{\rho}(0)G(x) - \widehat{(x\rho)}(0)G'(x), \quad x \in \mathbb{R} \quad (2.18)$$

and function $u_1(x)$ which satisfies the 1D Poisson equation with the far-field condition

$$-u_1''(x) = G_1(x), \quad x \in \mathbb{R}, \quad \lim_{x \rightarrow \pm\infty} \left[u_1(x) + \frac{1}{2} \left(\widehat{\rho}(0)|x| \mp \widehat{(x\rho)}(0) \right) \right] = 0. \quad (2.19)$$

Solving the above problem via the convolution, we have

$$u_1(x) = (U_{\text{Lap}} * G_1)(x) = \widehat{\rho}(0)u_{1,1}(x) - \widehat{(x\rho)}(0)u_{1,2}(x), \quad x \in \mathbb{R}, \quad (2.20)$$

where

$$u_{1,1}(x) = (U_{\text{Lap}} * G)(x) = -\frac{\sigma}{\sqrt{2\pi}} e^{-\frac{x^2}{2\sigma^2}} - \frac{1}{2} x \text{Erf}\left(\frac{x}{\sqrt{2}\sigma}\right), \quad (2.21)$$

$$u_{1,2}(x) = u'_{1,1}(x) = -\frac{1}{2} \text{Erf}\left(\frac{x}{\sqrt{2}\sigma}\right), \quad x \in \mathbb{R}. \quad (2.22)$$

Here, $\text{Erf}(x) = \frac{2}{\sqrt{\pi}} \int_0^x e^{-t^2} dt$ for $x \in \mathbb{R}$ is the error function. Combining (2.1) and (2.19), we solve the remaining function $u_2(x) = u(x) - u_1(x)$ via the Fourier integral:

$$\begin{aligned} u_2(x) &= (U_{\text{Lap}} * (\rho - G_1))(x) = \frac{1}{2\pi} \int_{\mathbb{R}} \frac{\widehat{\rho}(k) - \widehat{G}_1(k)}{k^2} e^{ikx} dk \quad (2.23) \\ &= \frac{1}{2\pi} \int_{\mathbb{R}} W(k) e^{ikx} dk \approx \frac{1}{2\pi} \int_{-P}^P W(k) e^{ikx} dk, \quad x \in \Omega(\mathbb{R}^2) \end{aligned}$$

where

$$W(k) = \begin{cases} \frac{\widehat{\rho}(k) - \widehat{G}_1(k)}{k^2} = \frac{\widehat{\rho}(k) - (\widehat{\rho}(0) + k(\widehat{\rho})'(0)) e^{-\frac{1}{2}k^2\sigma^2}}{k^2}, & k \neq 0, \\ -\frac{1}{2}(\widehat{x^2\rho})(0) + \frac{\sigma^2}{2}\widehat{\rho}(0), & k = 0, \end{cases} \quad k \in \mathbb{R} \quad (2.25)$$

Notice that the integrand $W(\mathbf{k})$ is smooth at the origin $k = 0$ in the Fourier space, therefore $u_2(x)$ can be computed by the regular FFT method. The choice of the parameter σ is similar as the one in the 2D case.

We remark that the 1D Poisson potential has also been dealt with successfully in [41] by plugging the Fourier spectral approximation of the density obtained on a finite interval, e.g. $[-L, L]$, into the convolution (1.2) formula. The method proposed there is an alternative good choice.

2.3 For confined Coulomb interactions

When $U(\mathbf{x})$ in (2.1) is taken as the confined Coulomb kernel $U_{\text{Con}}^\varepsilon(\mathbf{x})$ (1.12), there is no equivalent PDE formulation for the nonlocal potential $u(\mathbf{x})$.

When $d = 2$, noticing that

$$\widehat{U}_{\text{Con}}^\varepsilon(\mathbf{k}) \approx \begin{cases} \frac{1}{|\mathbf{k}|}, & |\mathbf{k}| \rightarrow 0, \\ \frac{\sqrt{2}}{\sqrt{\pi\varepsilon}|\mathbf{k}|^2}, & |\mathbf{k}| \rightarrow \infty, \end{cases} \quad \mathbf{k} \in \mathbb{R}^2, \quad (2.26)$$

we can immediately adapt the NUFFT-based solver [29] as follows:

$$\begin{aligned} u(\mathbf{x}) &= \frac{1}{(2\pi)^2} \int_{\mathbb{R}^2} e^{i\mathbf{k}\cdot\mathbf{x}} \widehat{U}_{\text{Con}}^\varepsilon(\mathbf{k}) \widehat{\rho}(\mathbf{k}) d\mathbf{k} \approx \frac{1}{(2\pi)^2} \int_{|\mathbf{k}| \leq P} e^{i\mathbf{k}\cdot\mathbf{x}} \widehat{U}_{\text{Con}}^\varepsilon(\mathbf{k}) \widehat{\rho}(\mathbf{k}) d\mathbf{k} \\ &= \frac{1}{(2\pi)^2} \int_0^P \int_0^{2\pi} e^{i\mathbf{k}\cdot\mathbf{x}} W_1(\mathbf{k}) \widehat{\rho}(\mathbf{k}) d|\mathbf{k}| d\theta, \quad \mathbf{x} \in \Omega \subset \mathbb{R}^2, \end{aligned} \quad (2.27)$$

where

$$W_1(\mathbf{k}) = |\mathbf{k}| \widehat{U}_{\text{Con}}^\varepsilon(\mathbf{k}) = \frac{2}{\pi} \int_0^\infty \frac{|\mathbf{k}| e^{-\frac{\varepsilon^2 s^2}{2}}}{|\mathbf{k}|^2 + s^2} ds = \begin{cases} \frac{2}{\pi} \int_0^\infty \frac{e^{-\varepsilon^2 |\mathbf{k}|^2 s^2 / 2}}{1+s^2} ds, & \mathbf{k} \neq \mathbf{0}, \\ 1, & \mathbf{k} = \mathbf{0}, \end{cases} \quad \mathbf{k} \in \mathbb{R}^2. \quad (2.28)$$

The integral in (2.28) can be evaluated very efficiently via the standard quadrature, such as the Gauss–Kronrod quadrature.

Similarly, when $d = 1$ (again we denote $\mathbf{k} = k$ and $\mathbf{x} = x$ for the scalar variables), noticing that

$$\widehat{U}_{\text{Con}}^\varepsilon(k) \approx \begin{cases} \frac{1}{2} [\ln 2 - \gamma_e - 2 \ln(\varepsilon |k|)], & |k| \rightarrow 0, \\ \frac{1}{\varepsilon^2 |k|^2}, & |k| \rightarrow \infty, \end{cases} \quad k \in \mathbb{R}, \quad (2.29)$$

we have

$$\begin{aligned} u(x) &= \frac{1}{2\pi} \int_{\mathbb{R}} e^{ikx} \widehat{U}_{\text{Con}}^\varepsilon(k) \widehat{\rho}(k) dk = -\frac{1}{2\pi} \int_{\mathbb{R}} e^{ikx} k \left[\partial_k \left(\widehat{U}_{\text{Con}}^\varepsilon(k) \widehat{\rho}(k) \right) + ix \widehat{U}_{\text{Con}}^\varepsilon(k) \widehat{\rho}(k) \right] dk \\ &= -\frac{1}{2\pi} \int_{\mathbb{R}} e^{ikx} \left[k \partial_k \widehat{U}_{\text{Con}}^\varepsilon(k) \widehat{\rho}(k) - ik \widehat{U}_{\text{Con}}^\varepsilon(k) (\widehat{x\rho})(k) + ixk \widehat{U}_{\text{Con}}^\varepsilon(k) \widehat{\rho}(k) \right] dk \\ &= \frac{1}{2\pi} \int_{\mathbb{R}} e^{ikx} \left[W_2(k) \widehat{\rho}(k) + i W_3(k) (\widehat{x\rho})(k) \right] dk - \frac{ix}{2\pi} \int_{\mathbb{R}} e^{ikx} W_3(k) \widehat{\rho}(k) dk \\ &\approx \frac{1}{2\pi} \int_{-P}^P e^{ikx} \left[W_2(k) \widehat{\rho}(k) + i W_3(k) (\widehat{x\rho})(k) \right] dk - \frac{ix}{2\pi} \int_{-P}^P e^{ikx} W_3(k) \widehat{\rho}(k) dk, \quad x \in [-L, L] \end{aligned} \quad (2.30)$$

Here

$$\begin{aligned} W_2(k) &= -k \partial_k \widehat{U}_{\text{Con}}^\varepsilon(k) = \int_0^\infty \frac{k^2 e^{-\varepsilon^2 s/2}}{(k^2 + s)^2} ds = \begin{cases} \int_0^\infty \frac{e^{-\varepsilon^2 k^2 s/2}}{(1+s)^2} ds, & k \neq 0, \\ 1, & k = 0, \end{cases} \quad k \in \mathbb{R}, \\ W_3(k) &= k \widehat{U}_{\text{Con}}^\varepsilon(k) = \int_0^\infty \frac{k e^{-\varepsilon^2 s/2}}{2(k^2 + s)} ds = \begin{cases} \int_0^\infty \frac{k e^{-\varepsilon^2 k^2 s/2}}{2(1+s)} ds, & k \neq 0, \\ 0, & k = 0, \end{cases} \quad k \in \mathbb{R}. \end{aligned} \quad (2.32)$$

The integrals in (2.31)-(2.32) can be evaluated very efficiently via the standard quadrature, and the integrals in (2.30) can be evaluated via the regular FFT.

Remark 2.1 *If $\rho(\mathbf{x})$ in (2.1) is spherically/radially symmetric in $3D/2D$, i.e. $\rho(\mathbf{x}) = \rho(|\mathbf{x}|) = \rho(r)$ with $r = |\mathbf{x}|$, and the interaction kernel $U(\mathbf{x})$ in (2.1) is taken as the Green's function of the Laplace operator in $3D/2D$, then the nonlocal interaction $u(\mathbf{x})$ in (2.1) is also spherically/radially symmetric in $3D/2D$, i.e. $u(\mathbf{x}) = u(|\mathbf{x}|) = u(r)$. Additionally, it satisfies the following second-order ODE*

$$-\frac{1}{r^{d-1}}\partial_r\left(r^{d-1}\partial_ru(r)\right)=\rho(r), \quad 0 < r < \infty, \quad d = 3, 2 \quad (2.33)$$

$$\partial_ru(0) = 0, \quad u(r) \rightarrow \begin{cases} 0, & d = 3, \\ -C_0 \ln r, & d = 2, \end{cases} \quad r \rightarrow \infty, \quad (2.34)$$

where $C_0 = \int_0^\infty \rho(r)r dr$. Moreover, if $\rho(r)$ has a compact support or decays exponentially fast when $r \rightarrow \infty$, the above problem can be further reformulated or approximated by [28, 35]

$$-\frac{1}{r^{d-1}}\partial_r\left(r^{d-1}\partial_ru(r)\right)=\rho(r), \quad 0 < r < L, \quad d = 3, 2, \quad (2.35)$$

$$\partial_ru(0) = 0, \quad \partial_ru(L) = \begin{cases} -\frac{u(L)}{L}, & d = 3, \\ \frac{u(L)}{L \ln L}, & d = 2, \end{cases} \quad (2.36)$$

where $L > 0$ is large enough such that $\text{supp}(\rho) \subset [0, L]$ or the truncation error in ρ outside $[0, L]$ can be negligible. This two-point boundary value problem can be solved by the finite difference (FDM) or finite element (FEM) or spectral method. Comparing to computing the original convolution or solving the corresponding Poisson equation in $3D/2D$, the memory and/or computational cost are significantly reduced.

2.4 Numerical comparisons

In order to demonstrate the efficiency and accuracy of the NUFFT for the evaluation of the nonlocal interaction (2.1) and compare it with other existing numerical methods, we adopt the error function

$$e_h := \frac{\|u - u_h\|_{l^\infty}}{\|u\|_{l^\infty}} = \frac{\max_{\mathbf{x} \in \Omega_h} |u(\mathbf{x}) - u_h(\mathbf{x})|}{\max_{\mathbf{x} \in \Omega_h} |u(\mathbf{x})|}, \quad (2.37)$$

where Ω_h represents the partition of the bounded computational domain Ω in 3D/2D with mesh size h and $u_h(\mathbf{x})$ is the numerical solution obtained by a numerical method on the domain Ω_h . We will compare the method via the NUFFT (referred as *NUFFT*) presented in this section with those existing numerical methods such as the method via the FFT (referred as *FFT*) [11] and via the DST (referred as *DST*) [17, 41] as well as the finite difference method via (2.35)-(2.36) (referred as *FDM*) [35] if it is possible.

Example 2.1. For the 3D Coulomb interaction, i.e. $d = 3$ and $U(\mathbf{x}) = U_{\text{Cou}}(\mathbf{x})$, we take $\rho(\mathbf{x}) := e^{-(x^2+y^2+\gamma^2 z^2)/\sigma^2}$ with $\sigma > 0$ and $\gamma \geq 1$. The 3D Coulomb interaction can be computed analytically as

$$u(\mathbf{x}) = \begin{cases} \frac{\sigma^3 \sqrt{\pi}}{4 |\mathbf{x}|} \text{Erf} \left(\frac{|\mathbf{x}|}{\sigma} \right), & \gamma = 1, \\ \frac{\sigma^2}{4\gamma} \int_0^\infty \frac{e^{-\frac{x^2+y^2}{\sigma^2(t+1)}} e^{-\frac{z^2}{\sigma^2(t+\gamma^2)}}}{(t+1)\sqrt{t+\gamma^2}} dt, & \gamma \neq 1, \end{cases} \quad \mathbf{x} \in \mathbb{R}^3. \quad (2.38)$$

The 3D Coulomb interaction $u(\mathbf{x})$ is computed numerically via the NUFFT, DST and FFT methods on a bounded computational domain $\Omega = [-L, L]^2 \times [-L/\gamma, L/\gamma]$ with mesh size h . Table 1 shows the errors e_h via the NUFFT, DST and FFT methods with $\gamma = 1, \sigma = 1.1$ for different mesh size h and L . Figure 1 depicts the error of the Coulomb interaction along the x -axis, which is defined as $\delta_h(x) := |u(x, 0, 0) - u_h(x, 0, 0)|$, obtained via the NUFFT and DST methods with $\gamma = 1, \sigma = 1.1$ for different mesh size h and L . In addition, Table 2 shows the errors e_h via the NUFFT, DST and FFT methods with $\sigma = 2$ and $L = 8, h = 1/4$ for different γ .

From Tables 1–2 and Figure 1, we can observe clearly that : (i) The errors are saturated in the DST and FFT methods as mesh size h tends smaller and the saturated accuracies decrease linearly with respect to the box size L ; (ii) The NUFFT method is spectrally accurate and it essentially does not depend on the domain, which implies that a very large bounded computational domain is not necessary in practical computations when the NUFFT method is used; (iii) The NUFFT is capable of dealing with anisotropic densities, which is quite useful in numerical simulation of BEC with strong confinement, while the errors by the DST and FFT methods increase dramatically with strongly anisotropic densities (cf. Tab. 2).

Example 2.2. For the 2D Coulomb interaction, i.e. $d = 2$ and $U(\mathbf{x}) = U_{\text{Cou}}(\mathbf{x})$, we take $\rho(\mathbf{x}) := e^{-(x^2+\gamma^2 y^2)/\sigma^2}$ with $\sigma > 0$ and $\gamma \geq 1$. The 2D

Table 1: Errors for the evaluation of the 3D Coulomb interaction by different methods for different h and L .

NUFFT	$h = 2$	$h = 1$	$h = 1/2$	$h = 1/4$	$h = 1/8$
$L = 4$	4.191E-01	2.696E-03	6.634E-07	4.599E-07	3.688E-07
$L = 8$	4.111E-01	2.817E-03	1.667E-08	2.367E-14	2.404E-14
$L = 16$	4.127E-01	2.848E-03	1.732E-08	1.420E-14	1.334E-14
DST	$h = 2$	$h = 1$	$h = 1/2$	$h = 1/4$	$h = 1/8$
$L = 4$	2.437E-01	2.437E-01	2.437E-01	2.437E-01	2.437E-01
$L = 8$	2.754E-01	1.219E-01	1.219E-01	1.219E-01	1.219E-01
$L = 16$	3.433E-01	6.093E-02	6.093E-02	6.093E-02	6.093E-02
$L = 32$	3.780E-01	3.046E-02	3.046E-02	3.046E-02	3.046E-02
$L = 64$	3.956E-01	1.523E-02	1.523E-02	1.523E-02	1.523E-02
FFT	$h = 2$	$h = 1$	$h = 1/2$	$h = 1/4$	$h = 1/8$
$L = 4$	3.032E-01	3.363E-01	3.385E-01	3.385E-01	3.385E-01
$L = 8$	1.744E-01	1.712E-01	1.720E-01	1.720E-01	1.720E-01
$L = 16$	2.958E-01	8.666E-02	8.632E-02	8.632E-02	8.632E-02
$L = 32$	3.550E-01	4.372E-02	4.320E-02	4.320E-02	4.320E-02
$L = 64$	3.843E-01	2.214E-02	2.161E-02	2.161E-02	2.161E-02

Table 2: Errors for the evaluation of the 3D Coulomb interaction by different methods with $\sigma = 2$ and $L = 8, h = 1/4$ for different γ .

	$\gamma = 1$	$\gamma = 2$	$\gamma = 4$	$\gamma = 8$
NUFFT	2.164E-14	2.134E-14	2.044E-14	2.005E-14
DST	0.146	0.441	1.559	3.782
FFT	0.208	0.310	1.327	3.349

Coulomb interaction can be obtained analytically as

$$u(\mathbf{x}) = \begin{cases} \frac{\sqrt{\pi}\sigma}{2} I_0\left(\frac{|\mathbf{x}|^2}{2\sigma^2}\right) e^{-\frac{|\mathbf{x}|^2}{2\sigma^2}}, & \gamma = 1, \\ \frac{\sigma}{\gamma\sqrt{\pi}} \int_0^\infty \frac{e^{-\frac{x^2}{\sigma^2(t^2+1)}} e^{-\frac{y^2}{\sigma^2(t^2+\gamma^{-2})}}}{\sqrt{t^2+1}\sqrt{t^2+\gamma^{-2}}} dt, & \gamma \neq 1, \end{cases} \quad \mathbf{x} \in \mathbb{R}^2, \quad (2.39)$$

where I_0 is the modified Bessel function of order zero [1]. To numerically

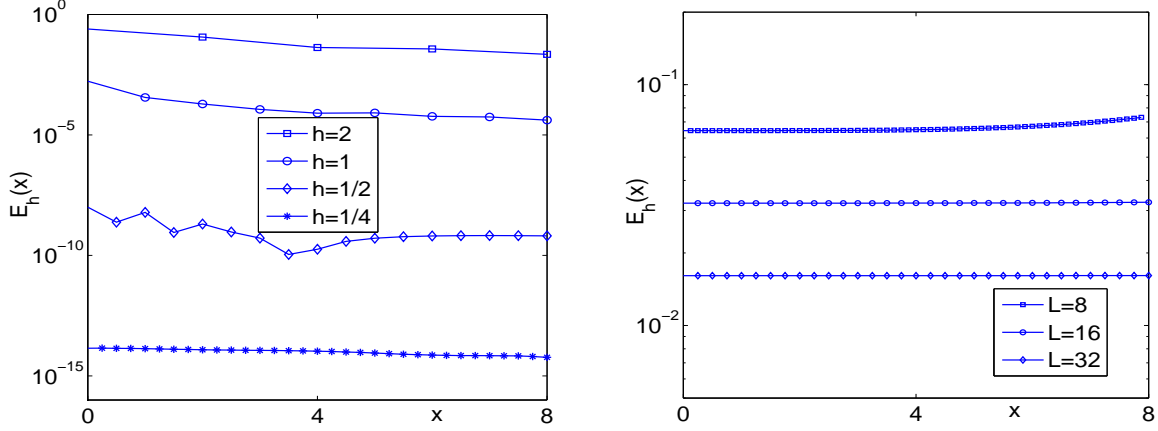


Figure 1: Errors of $\delta_h(x) = |u(x, 0, 0) - u_h(x, 0, 0)|$ for the evaluation of the Coulomb interaction in 3D via the NUFFT method with $L = 8$ for different mesh size h (left) and via the DST method with mesh size $h = 1/4$ for different L (right).

compute the integral in (2.39), we can first split it into two integrals and reformulate the one with infinite interval into some equivalent integral with finite interval by a simple change of variable. Then, we apply Gauss–Kronrod quadrature to each with fine accuracy control so as to achieve accurate reference solutions.

The 2D Coulomb interaction $u(\mathbf{x})$ is computed numerically via the NUFFT, DST and FFT methods on a bounded computational domain $\Omega = [-L, L] \times [-L/\gamma, L/\gamma]$ with mesh size h . Table 3 shows the errors e_h via the NUFFT, DST and FFT methods with $\sigma = \sqrt{1.2}$ and $\gamma = 1$ under different mesh size h and L . In addition, Table 4 shows the errors e_h via the NUFFT, DST and FFT methods with $\sigma = 2$, $L = 12$ and $h = 1/8$ for different γ .

From Tables 3-4, we can conclude that: (i) The errors obtained by the DST and FFT methods reach a saturation accuracy on any fixed domain and we can observe a first order convergence in the saturated accuracy with respect to the domain size L . (ii) The NUFFT method is spectrally accurate and it essentially does not depend on the domain which makes it perfect for computing the free space potential. (iii) The NUFFT is capable of dealing with anisotropic densities, while the results obtained by the DST and FFT methods are far from the exact solutions when the bounded computational domain is not large enough.

Table 3: Errors for the evaluation of the 2D Coulomb interaction by different methods for different h and L .

NUFFT	$h = 2$	$h = 1$	$h = 1/2$	$h = 1/4$	$h = 1/8$
$L = 4$	1.837	5.540E-02	4.289E-07	3.383E-07	2.937E-07
$L = 8$	4.457E-01	2.373E-03	2.714E-08	3.202E-15	3.431E-15
$L = 16$	2.084E-01	2.385E-03	2.761E-08	2.745E-15	2.859E-15
DST	$h = 2$	$h = 1$	$h = 1/2$	$h = 1/4$	$h = 1/8$
$L = 4$	1.577E-01	1.577E-01	1.577E-01	1.577E-01	1.577E-01
$L = 8$	1.348E-01	7.762E-02	7.762E-02	7.762E-02	7.762E-02
$L = 16$	1.711E-01	3.867E-02	3.867E-02	3.867E-02	3.867E-02
$L = 32$	1.897E-01	1.932E-02	1.932E-02	1.932E-02	1.932E-02
$L = 64$	1.991E-01	9.658E-03	9.658E-03	9.658E-03	9.658E-03
FFT	$h = 2$	$h = 1$	$h = 1/2$	$h = 1/4$	$h = 1/8$
$L = 4$	2.855E-01	2.961E-01	2.980E-01	2.980E-01	2.980E-01
$L = 8$	1.553E-01	1.503E-01	1.502E-01	1.502E-01	1.502E-01
$L = 16$	1.157E-01	7.596E-02	7.528E-02	7.528E-02	7.528E-02
$L = 32$	1.624E-01	3.843E-02	3.766E-02	3.766E-02	3.766E-02
$L = 64$	1.856E-01	1.961E-02	1.883E-02	1.883E-02	1.883E-02

Table 4: Errors for the evaluation of the 2D Coulomb interaction by different methods with $L = 12, h = 1/8$ for different γ .

	$\gamma = 1$	$\gamma = 2$	$\gamma = 4$	$\gamma = 8$
NUFFT	4.230E-14	3.102E-15	3.504E-15	4.381E-15
DST	0.373	0.386	0.412	0.446
FFT	0.426	0.425	0.405	0.344

Example 2.3. For the 2D Poisson potential, i.e. $d = 2$ and $U(\mathbf{x}) = U_{\text{Lap}}(\mathbf{x})$, we take $\rho(\mathbf{x}) := e^{-|\mathbf{x}|^2/\sigma^2} = e^{-r^2/\sigma^2}$ with $r = |\mathbf{x}|$ and $\sigma > 0$. The 2D Poisson potential can be obtained analytically as

$$u(\mathbf{x}) = -\frac{\sigma^2}{4} \left[\text{E}_1 \left(\frac{|\mathbf{x}|^2}{\sigma^2} \right) + 2 \ln(|\mathbf{x}|) \right], \quad \mathbf{x} \in \mathbb{R}^2. \quad (2.40)$$

In this case, we choose $\sigma = \sqrt{1.3}$. The 2D Poisson potential $u(\mathbf{x})$ is

computed numerically via the NUFFT method on a bounded computational domain $\Omega = [-L, L]^2$ with mesh size h and the FDM through the formulation (2.35)-(2.36) on the interval $[0, L]$ with mesh size h .

Table 5 shows the errors of the 2D Poisson potential obtained by the NUFFT solver on a square domain and the errors by the FDM solver as well as its convergence rate with respect to the mesh size h . In addition, to demonstrate the efficiency of the NUFFT method, Table 6 displays the computational time (CPU time in seconds) of the NUFFT solver with $L = 16$ and $h = 1/4$, where the time is measured when the algorithm is implemented in Fortran, the code is compiled by ifort 13.1.2 using the option -g, and executed on 32-bit Ubuntu Linux on a 2.90GHz Intel(R) Core(TM) i7-3520M CPU with 6MB cache.

Table 5: Errors for the evaluation of the 2D Poisson potential by different methods for different h and L .

NUFFT	$h = 2$	$h = 1$	$h = 1/2$	$h = 1/4$	$h = 1/8$
$L = 4$	5.821E-01	1.133E-02	3.011E-06	1.994E-06	1.650E-06
$L = 8$	1.685E-01	6.820E-04	1.754E-09	4.936E-14	4.857E-14
$L = 16$	1.684E-01	5.333E-04	1.391E-09	4.577E-14	4.561E-14
FDM	$h = 1/4$	$h = 1/8$	$h = 1/16$	$h = 1/32$	$h = 1/64$
$L = 4$	4.646E-03	1.155E-03	2.910E-04	7.602E-05	2.246E-05
rate	-	2.0081	1.9889	1.9365	1.7590
$L = 8$	4.101E-03	1.019E-03	2.542E-04	6.353E-05	1.588E-05
rate	-	2.0093	2.0024	2.0006	2.0002
$L = 16$	4.052E-03	1.007E-03	2.512E-04	6.278E-05	1.569E-05
rate	-	2.0092	2.0023	2.0006	2.0001

From Tables 5–6, we can see clearly that: (i) The NUFFT solver is spectrally accurate while the FDM solver is only second order accurate, and the NUFFT solver is much more accurate than the FDM solver. (ii) The errors obtained by both methods do not essentially depend on the domain size; (iii) The complexity of the NUFFT solver scales like $O(N \ln N)$ as expected, which is the same as those presented in [29].

Table 6: CPU time (in seconds) of the NUFFT solver for the evaluation of the 2D Poisson potential. Here T_{FFT} and T_{NUFFT} are the time for the evaluation of I_1 and I_2 in (2.3) via the FFT and NUFFT methods, respectively.

Time	T_{FFT}	T_{NUFFT}	T_{Total}
$h = 1$	0.01	0.05	0.06
$h = 1/2$	0.02	0.08	0.10
$h = 1/4$	0.12	0.20	0.32
$h = 1/8$	0.60	0.78	1.38

3 Computing the ground state

In this section, we present an efficient and accurate numerical method for computing the ground state of (1.13) by combining NUFFT-based nonlocal interaction potential solver and the normalized gradient flow that is discretised by backward Euler Fourier pseudospectral method, and compare it with those existing numerical methods.

3.1 A numerical method via the NUFFT

We choose $\tau > 0$ as the time step and denote $t_n = n\tau$ for $n = 0, 1, 2, \dots$. Different efficient and accurate numerical methods have been proposed in the literature for computing the ground state [6, 7, 8, 21, 41]. One of the most simple and popular methods is through the following gradient flow with discretized normalization (GFDN):

$$\begin{aligned} \partial_t \phi(\mathbf{x}, t) &= \left[\frac{1}{2} \Delta - V(\mathbf{x}) - \beta \varphi(\mathbf{x}, t) \right] \phi(\mathbf{x}, t), & \mathbf{x} \in \mathbb{R}^d, \quad t_n \leq t < t_{n+1}, \\ \varphi(\mathbf{x}, t) &= (U * |\phi|^2)(\mathbf{x}, t), & \mathbf{x} \in \mathbb{R}^d, \quad t_n \leq t < t_{n+1}, \end{aligned} \quad (3.2)$$

$$\phi(\mathbf{x}, t_{n+1}) := \phi(\mathbf{x}, t_{n+1}^+) = \frac{\phi(\mathbf{x}, t_{n+1}^-)}{\|\phi(\mathbf{x}, t_{n+1}^-)\|}, \quad \mathbf{x} \in \mathbb{R}^d, \quad n = 0, 1, 2, \dots \quad (3.3)$$

with the initial data

$$\phi(\mathbf{x}, 0) = \phi_0(\mathbf{x}), \quad \mathbf{x} \in \mathbb{R}^d, \quad \text{with} \quad \|\phi_0\|^2 := \int_{\mathbb{R}^d} |\phi_0(\mathbf{x})|^2 d\mathbf{x} = 1. \quad (3.4)$$

Let $\phi^n(\mathbf{x})$ and $\varphi^n(\mathbf{x})$ be the numerical approximation of $\phi(\mathbf{x}, t_n)$ and $\varphi(\mathbf{x}, t_n)$, respectively, for $n \geq 0$. The above GFDN is usually discretized in time via the backward Euler method [6, 7, 8, 21, 41]

$$\frac{\phi^{(1)}(\mathbf{x}) - \phi^n(\mathbf{x})}{\tau} = \left[\frac{1}{2} \Delta - V(\mathbf{x}) - \beta \varphi^n(\mathbf{x}) \right] \phi^{(1)}(\mathbf{x}), \quad \mathbf{x} \in \mathbb{R}^d \quad (3.5)$$

$$\varphi^n(\mathbf{x}) = (U * |\phi^n|^2)(\mathbf{x}), \quad \mathbf{x} \in \mathbb{R}^d, \quad (3.6)$$

$$\phi^{n+1}(\mathbf{x}) = \frac{\phi^{(1)}(\mathbf{x})}{\|\phi^{(1)}(\mathbf{x})\|}, \quad \mathbf{x} \in \mathbb{R}^d, \quad n = 0, 1, 2, \dots \quad (3.7)$$

Then an efficient and accurate numerical method can be designed by: (i) truncating the above problem on a bounded computational domain Ω with periodic BC on $\partial\Omega$; (ii) discretizing in space via the Fourier pseudospectral method; and (iii) evaluating the nonlocal interaction $\varphi^n(\mathbf{x})$ in (3.6) by the algorithm via the NUFFT discussed in the previous section. When $\phi_0(\mathbf{x})$ is chosen as a positive function, the ground state can be obtained as $\phi_g(\mathbf{x}) = \lim_{n \rightarrow \infty} \phi^n(\mathbf{x})$ for $\mathbf{x} \in \Omega$. The details are omitted here for brevity and this method is referred as the *GF-NUFFT* method. We remark here that $|\phi^n|^2(\mathbf{0}) = 1$ for $n \geq 0$.

For comparison, for the Coulomb interaction in 3D/2D, when the NUFFT solver is replaced by the standard FFT, we refer the method as *GF-FFT*. In addition, when (3.6) is reformulated as its equivalent PDE formulation (1.7)-(1.8) on Ω with homogeneous Dirichlet BC on $\partial\Omega$ and solved via the sine pseudospectral method [6, 9, 41], we refer it as *GF-DST*.

3.2 Numerical comparisons

In order to compare the *GF-NUFFT* method with *GF-FFT* and *GF-DST* methods for computing the ground state, we denote $\varphi_g(\mathbf{x}) = (U * \phi_g)(\mathbf{x})$ and introduce the errors

$$e_{\phi_g}^h := \frac{\max_{\mathbf{x} \in \Omega^h} |\phi_g(\mathbf{x}) - \phi_g^h(\mathbf{x})|}{\max_{\mathbf{x} \in \Omega^h} |\phi_g(\mathbf{x})|}, \quad e_{\varphi_g}^h := \frac{\max_{\mathbf{x} \in \Omega^h} |\varphi_g(\mathbf{x}) - \varphi_g^h(\mathbf{x})|}{\max_{\mathbf{x} \in \Omega^h} |\varphi_g(\mathbf{x})|},$$

where ϕ_g^h and φ_g^h are obtained numerically by a numerical method with mesh size h . Additionally, we split the energy functional into three parts

$$E(\phi) = E_{\text{kin}}(\phi) + E_{\text{pot}}(\phi) + E_{\text{int}}(\phi),$$

where the kinetic energy $E_{\text{kin}}(\phi)$, the potential energy $E_{\text{pot}}(\phi)$ and the interaction energy $E_{\text{int}}(\phi)$ are defined as

$$E_{\text{kin}}(\phi) = \frac{1}{2} \int_{\mathbb{R}^d} |\nabla \phi(\mathbf{x})|^2 d\mathbf{x}, \quad E_{\text{pot}}(\phi) = \int_{\mathbb{R}^d} V(\mathbf{x}) |\phi(\mathbf{x})|^2 d\mathbf{x}, \quad E_{\text{int}}(\phi) = \frac{\beta}{2} \int_{\mathbb{R}^d} \varphi(\mathbf{x}) |\phi(\mathbf{x})|^2 d\mathbf{x},$$

respectively. Moreover, the chemical potential can be reformulated as $\mu(\phi) = E(\phi) + E_{\text{int}}(\phi)$. Furthermore, if the external potential $V(\mathbf{x})$ in (1.1) was taken as the harmonic potential [4, 9, 35], the energies of the ground state satisfy the following virial identity

$$0 = I := 2E_{\text{kin}}(\phi_g) - 2E_{\text{pot}}(\phi_g) + \begin{cases} E_{\text{int}}(\phi_g), & U = U_{\text{Cou}} \text{ in } 3\text{D}/2\text{D}, \\ \frac{\beta}{4\pi}, & U = U_{\text{Lap}} \text{ in } 2\text{D}. \end{cases}$$

We denote I^h as an approximation of I when ϕ_g is replaced by ϕ_g^h in the above equality. In our computations, the ground state ϕ_g^h is reached numerically when $\max_{\mathbf{x} \in \Omega^h} \frac{|\phi^{n+1}(\mathbf{x}) - \phi^n(\mathbf{x})|}{\tau} \leq \varepsilon_0$ with ε_0 a prescribed accuracy, e.g. $\varepsilon_0 = 10^{-10}$. The initial data $\phi_0(\mathbf{x})$ is chosen as a Gaussian and the time step is taken as $\tau = 10^{-2}$. In the comparisons, the ‘‘exact’’ solution $\phi_g(\mathbf{x})$ was obtained numerically via the GF-NUFFT method on a large enough domain Ω with small enough mesh size h and time step τ .

Example 3.1. *For the NLSE with the Coulomb interaction in 3D*, i.e. we take $d = 3$ and $U(\mathbf{x}) = U_{\text{Cou}}(\mathbf{x})$ in (1.1)-(1.2). The ground state is computed numerically on a bounded domain $\Omega = [-8, 8]^3$. Table 7 shows the errors $e_{\phi_g}^h$ and $e_{\varphi_g}^h$ with $V(\mathbf{x}) = \frac{1}{2}(x^2 + y^2 + z^2)$ in (1.1) for different numerical methods, β and mesh size h . In addition, Table 8 lists the energy $E_g := E(\phi_g^h)$, chemical potential $\mu_g := \mu(\phi_g^h)$, kinetic energy $E_{\text{kin}}^g := E_{\text{kin}}(\phi_g^h)$, potential energy $E_{\text{pot}}^g := E_{\text{pot}}(\phi_g^h)$, interaction energy $E_{\text{int}}^g := E_{\text{int}}(\phi_g^h)$ and I^h with $h = 1/8$ and $V(\mathbf{x}) = \frac{1}{2}(x^2 + y^2 + 4z^2)$ in (1.1) for different β .

Example 3.2 *For the NLSE with the Coulomb interaction in 2D*, i.e. we take $d = 2$ and $U(\mathbf{x}) = U_{\text{Cou}}(\mathbf{x})$ in (1.1)-(1.2). The ground state is computed numerically on a bounded domain $\Omega = [-L, L]^2$ with different mesh size h . Table 9 shows the errors $e_{\phi_g}^h$ and $e_{\varphi_g}^h$ with $V(\mathbf{x}) = \frac{1}{2}(x^2 + 4y^2)$ for different numerical methods, β and mesh size h on $[-L, L]^2$. In addition, Table 10 lists the energy $E_g := E(\phi_g^h)$, chemical potential $\mu_g := \mu(\phi_g^h)$, kinetic energy $E_{\text{kin}}^g := E_{\text{kin}}(\phi_g^h)$, potential energy $E_{\text{pot}}^g := E_{\text{pot}}(\phi_g^h)$, interaction energy $E_{\text{int}}^g := E_{\text{int}}(\phi_g^h)$ and I^h with $h = 1/8$ and $V(\mathbf{x}) = \frac{1}{2}(x^2 + 4y^2)$ on $[-8, 8]^2$ for different β .

Example 3.3 *For the NLSE with the Poisson potential in 2D*, i.e. we take $d = 2$ and $U(\mathbf{x}) = U_{\text{Lap}}(\mathbf{x})$ in (1.1)-(1.2). The ground state is computed numerically on a bounded domain $\Omega = [-8, 8]^2$ with different mesh size h . Table 11 shows the errors $e_{\phi_g}^h$ and $e_{\varphi_g}^h$ with $V(\mathbf{x}) = \frac{1}{2}(x^2 + 4y^2)$ in (1.1)

Table 7: Errors of the ground state for the NLSE with the 3D Coulomb interaction for different methods and mesh size h .

GF-NUFFT		$h = 2$	$h = 1$	$h = 1/2$	$h = 1/4$
$e_{\phi_g}^h$	$\beta = -5$	5.362E-02	1.954E-04	2.201E-07	4.643E-11
	$\beta = 5$	1.512E-01	4.712E-04	4.026E-08	1.141E-10
$e_{\varphi_g}^h$	$\beta = -5$	2.532E-01	3.769E-03	8.153E-07	7.035E-11
	$\beta = 5$	2.682E-01	7.061E-04	1.225E-07	8.048E-11
GF-DST		$h = 2$	$h = 1$	$h = 1/2$	$h = 1/4$
$e_{\phi_g}^h$	$\beta = -5$	2.319E-01	9.439E-03	1.637E-06	6.309E-07
	$\beta = 5$	1.659E-01	9.469E-04	8.306E-07	8.531E-07
$e_{\varphi_g}^h$	$\beta = -5$	7.297E-02	9.551E-02	9.945E-02	1.027E-01
	$\beta = 5$	7.809E-02	1.016E-01	1.057E-01	1.091E-01

for different numerical methods, β and mesh size h . In addition, Table 12 lists the energy $E_g := E(\phi_g^h)$, chemical potential $\mu_g := \mu(\phi_g^h)$, kinetic energy $E_{\text{kin}}^g := E_{\text{kin}}(\phi_g^h)$, potential energy $E_{\text{pot}}^g := E_{\text{pot}}(\phi_g^h)$, interaction energy $E_{\text{int}}^g := E_{\text{int}}(\phi_g^h)$ and I^h with $h = 1/8$ and $V(\mathbf{x}) = \frac{1}{2}(x^2 + 4y^2)$ in (1.1) for different β .

From Tables 7-12 and additional numerical results not shown here for brevity, we can see that: (i) The *GF-NUFFT* method is spectrally accurate in space, while the *GF-DST* method has a saturation accuracy for a fixed domain; (ii) The saturation error of the *GF-DST* depends inversely on the domain size L , and it can only reach satisfactory accuracy for some large L ; (iii) High accuracy, i.e., 9-digits accurate, is achieved by *GF-NUFFT* as quite expected in the energies, which, in another way, manifest the high-accuracy advantage of our NUFFT solver.

4 For computing the dynamics

In this section, we present an efficient and accurate numerical method for computing the dynamics of the NLSE with the nonlocal interaction potential (1.1)-(1.2) and the initial data (1.3) by combining the NUFFT solver for the nonlocal interaction potential evaluation and the time-splitting Fourier pseudospectral discretization, and compare it with those existing numerical methods.

Table 8: Different energies of the ground state and I^h for the NLSE with the 3D Coulomb interaction for different β .

β	E_g	μ_g	E_{kin}^g	E_{pot}^g	E_{int}^g	I^h
-10	1.6370	1.2630	1.0990	9.1197E-01	-3.7401E-01	-3.39E-10
-5	1.8212	1.6397	1.0467	9.5594E-01	-1.8147E-01	-3.63E-10
-1	1.9646	1.9292	1.0089	9.9118E-01	-3.5462E-02	-3.87E-10
1	2.0351	2.0702	9.9128E-01	1.0088	3.5064E-02	-3.86E-10
5	2.1739	2.3454	9.5831E-01	1.0441	1.7151E-01	-4.30E-10
10	2.3431	2.6772	9.2101E-01	1.0880	3.3408E-01	-1.16E-10

Table 9: Errors of the ground state for the NLSE with 2D Coulomb interaction on $[-L, L]^2$ with mesh size h .

GF-NUFFT ($L = 8$)		$h = 1$	$h = 1/2$	$h = 1/4$	$h = 1/8$
$e_{\phi_g}^h$	$\beta = -5$	4.620E-02	1.058E-03	5.570E-08	3.968E-15
	$\beta = 5$	7.034E-03	2.365E-05	2.632E-10	2.074E-15
$e_{\varphi_g}^h$	$\beta = -5$	1.025E-01	1.402E-03	8.244E-08	4.445E-15
	$\beta = 5$	1.263E-02	3.239E-05	3.161E-10	1.703E-15
GF-DST ($L = 8$)		$h = 1$	$h = 1/2$	$h = 1/4$	$h = 1/8$
$e_{\phi_g}^h$	$\beta = -5$	4.823E-02	1.112E-03	3.139E-05	3.133E-05
	$\beta = 5$	8.183E-03	7.245E-05	5.317E-05	5.381E-05
$e_{\varphi_g}^h$	$\beta = -5$	6.613E-02	5.159E-02	5.159E-02	5.159E-02
	$\beta = 5$	6.840E-02	6.840E-02	6.840E-02	6.840E-02
GF-DST ($h = 1/8$)		$L = 8$	$L = 16$	$L = 32$	$L = 64$
$e_{\phi_g}^h$	$\beta = -5$	3.133E-05	3.848E-06	4.789E-07	5.980E-08
	$\beta = 5$	5.381E-05	6.212E-06	7.606E-07	9.445E-08
$e_{\varphi_g}^h$	$\beta = -5$	5.159E-02	2.572E-02	1.072E-02	5.248E-03
	$\beta = 5$	6.840E-02	3.398E-02	1.415E-02	6.928E-03

4.1 A numerical method via the NUFFT

From time $t = t_n$ to $t = t_{n+1}$, the NLSE (1.1) will be solved in two splitting steps. One solves first

$$i \partial_t \psi(\mathbf{x}, t) = -\frac{1}{2} \Delta \psi(\mathbf{x}, t), \quad \mathbf{x} \in \mathbb{R}^d, \quad t_n \leq t \leq t_{n+1}, \quad (4.1)$$

Table 10: Different energies of the ground state and I^h for the NLSE with the 2D Coulomb interaction for different β .

β	E_g	μ_g	E_{kin}^g	E_{pot}^g	E_{int}^g	I^h
-10	0.1367	-1.4536	1.2611	4.6592E-01	-1.5903	1.89E-10
-5	0.8698	0.1933	9.4226E-01	6.0401E-01	-6.7651E-01	2.37E-10
-1	1.3808	1.2600	7.8098E-01	7.2058E-01	-1.2080E-01	2.60E-10
1	1.6163	1.7311	7.2201E-01	7.7942E-01	1.1483E-01	-2.61E-10
5	2.0551	2.5801	6.3379E-01	8.9629E-01	5.2501E-01	-2.65E-10
10	2.5557	3.5132	5.5977E-01	1.0385	9.5748E-01	-2.69E-10

Table 11: Errors of the ground state for the NLSE with the 2D Poisson potential with mesh size h .

GF-NUFFT		$h = 1$	$h = 1/2$	$h = 1/4$	$h = 1/8$
$e_{\phi_g}^h$	$\beta = -5$	2.465E-02	1.024E-04	4.699E-10	2.878E-15
	$\beta = 5$	1.191E-02	1.593E-05	9.793E-12	2.726E-15
$e_{\varphi_g}^h$	$\beta = -5$	3.737E-02	7.634E-05	2.896E-10	6.347E-14
	$\beta = 5$	1.033E-02	3.282E-06	2.682E-12	6.247E-14

for the time step of length τ , followed by solving

$$i \partial_t \psi(\mathbf{x}, t) = [V(\mathbf{x}) + \beta \varphi(\mathbf{x}, t)] \psi(\mathbf{x}, t), \quad \varphi(\mathbf{x}, t) = (U * |\psi|^2)(\mathbf{x}, t), \quad \mathbf{x} \in \mathbb{R}^d, \quad t_n \leq t \leq t_{n+1}, \quad (4.2)$$

for the same time step. For $t \in [t_n, t_{n+1}]$, Eq. (4.2) leaves $|\psi|$ invariant in t [5, 9], i.e. $|\psi(\mathbf{x}, t)| = |\psi(\mathbf{x}, t_n)|$, and thus φ is time invariant, i.e. $\varphi(\mathbf{x}, t) = \varphi(\mathbf{x}, t_n) := \varphi^n(\mathbf{x})$, therefore it becomes

$$i \partial_t \psi(\mathbf{x}, t) = [V(\mathbf{x}) + \beta \varphi^n(\mathbf{x})] \psi(\mathbf{x}, t), \quad \varphi^n(\mathbf{x}) = (U * |\psi^n|^2)(\mathbf{x}), \quad \mathbf{x} \in \mathbb{R}^d, \quad t_n \leq t \leq t_{n+1}, \quad (4.3)$$

where $\psi^n(\mathbf{x}) := \psi(\mathbf{x}, t_n)$, which immediately implies that

$$\psi(\mathbf{x}, t) = e^{-i[V(\mathbf{x}) + \beta \varphi^n(\mathbf{x})](t-t_n)} \psi(\mathbf{x}, t_n), \quad \mathbf{x} \in \mathbb{R}^d, \quad t_n \leq t \leq t_{n+1}. \quad (4.4)$$

Table 12: Different energies of the ground state and I^h for the NLSE with the 2D Poisson potential for different β .

β	E_g	μ_g	E_{kin}^g	E_{pot}^g	E_{int}^g	I^h
-10	1.3533	1.1432	9.8061E-01	5.8272E-01	-2.1008E-01	2.44E-10
-5	1.4429	1.3691	8.5784E-01	6.5889E-01	-7.3819E-02	2.54E-10
-1	1.4913	1.4819	7.7024E-01	7.3045E-01	-9.3826E-03	2.59E-10
1	1.5073	1.5139	7.3046E-01	7.7025E-01	6.5762E-03	-2.62E-10
5	1.5221	1.5260	6.5959E-01	8.5854E-01	3.9516E-03	-2.70E-10
10	1.5076	1.4420	5.8770E-01	9.8559E-01	-6.5660E-02	-2.81E-10

Then an efficient and accurate numerical method can be designed by: (i) adopting a second-order Strang splitting [38] or a fourth-order time splitting method [40] to decouple the nonlinearity; (ii) truncating the problem on a bounded computational domain Ω , and imposing the periodic BC on $\partial\Omega$ for the subproblem (4.1); (iii) discretizing (4.1) in space by the Fourier spectral method and integrating in time *exactly*; (iv) evaluating the nonlocal interaction $\varphi^n(\mathbf{x})$ in (4.4) by the algorithm via the NUFFT that discussed in previous sections, and integrating in time *exactly* for (4.4). The details are omitted here for brevity and this method is referred as the *TS-NUFFT* method.

For comparison, for the nonlocal interaction in 3D/2D, when the NUFFT in the above method is replaced by the standard FFT, we refer the method as *TS-FFT*. In addition, when the nonlocal interaction $\varphi^n(\mathbf{x})$ in (4.4) is reformulated as its equivalent PDE formulation (1.7)-(1.8) on Ω with homogeneous Dirichlet BC on $\partial\Omega$ and then discretized by the sine pseudospectral method with an evaluation of (4.1) via the sine spectral method and integrated in time *exactly* [6, 41], we refer it as *TS-DST*.

4.2 Numerical comparisons

Again, in order to compare the *TS-NUFFT* method with the *GF-DST* method for computing the dynamics, we denote $\rho(\mathbf{x}, t) = |\psi(\mathbf{x}, t)|^2$ and

$\varphi(\mathbf{x}, t) = (U * |\psi|^2)(\mathbf{x}, t)$ and introduce the errors

$$\begin{aligned} e_{\psi}^h(t) &:= \frac{\max_{\mathbf{x} \in \Omega^h} |\psi(\mathbf{x}, t) - \psi_h^n(\mathbf{x})|}{\max_{\mathbf{x} \in \Omega^h} |\psi(\mathbf{x}, t)|}, & e_{\varphi}^h(t) &:= \frac{\max_{\mathbf{x} \in \Omega^h} |\varphi(\mathbf{x}, t) - \varphi_h^n(\mathbf{x})|}{\max_{\mathbf{x} \in \Omega^h} |\varphi(\mathbf{x}, t)|}, \\ e_{\rho}^h(t) &:= \frac{\max_{\mathbf{x} \in \Omega^h} |\rho(\mathbf{x}, t) - \rho_h^n(\mathbf{x})|}{\max_{\mathbf{x} \in \Omega^h} |\rho(\mathbf{x}, t)|}, & t = t_n, \quad n \geq 0, \end{aligned}$$

where $\psi_h^n(\mathbf{x})$, $\varphi_h^n(\mathbf{x})$ and $\rho_h^n(\mathbf{x})$ are obtained numerically by a numerical method as the approximations of $\psi(\mathbf{x}, t)$, $\varphi(\mathbf{x}, t)$ and $\rho(\mathbf{x}, t)$ at $t = t_n$, respectively with a given mesh size h and a very small time step $\tau > 0$. The external potential in (1.1) and the initial data in (1.3) are chosen as

$$V(\mathbf{x}) = \frac{|\mathbf{x}|^2}{2}, \quad \psi(\mathbf{x}, 0) = \psi_0(\mathbf{x}) = e^{-\frac{|\mathbf{x}|^2}{2}}, \quad \mathbf{x} \in \mathbb{R}^d \text{ with } d = 3 \text{ or } 2. \quad (4.5)$$

In the comparisons, the ‘‘exact’’ solution $\psi(\mathbf{x}, t)$ (and thus $\varphi(\mathbf{x}, t)$ and $\rho(\mathbf{x}, t)$) was obtained numerically via the TS-NUFFT method on a large enough domain Ω with very small enough mesh size h and time step τ . In our computations, we use the fourth-order time-splitting method for time integration [40].

Example 4.1 *For the NLSE with the 3D Coulomb interaction, i.e. $d = 3$ and $U(\mathbf{x}) = U_{\text{Cou}}(\mathbf{x})$ in (1.1)-(1.2). The problem is solved numerically on a bounded computational domain $\Omega = [-8, 8]^3$ with time step $\tau = 10^{-3}$ and different mesh size h . Table 13 list the errors of the wave-function, the density and the 3D Coulomb interaction at $t = 1/8$ obtained by the TS-NUFFT and TS-DST methods for different mesh size h and interaction constant β .*

Example 4.2 *For the NLSE with the 2D Coulomb interaction, i.e. $d = 2$ and $U(\mathbf{x}) = U_{\text{Cou}}(\mathbf{x})$ in (1.1)-(1.2). The problem is solved numerically on a bounded computational domain $\Omega = [-16, 16]^2$ with time step $\tau = 10^{-4}$ and different mesh size h . Table 14 shows the errors of the wave-function and the 2D Coulomb interaction at $t = 0.5$ obtained by the TS-NUFFT and TS-DST methods for different mesh size h and interaction constant β .*

Example 4.3 *For the NLSE with the 2D Poisson potential, i.e. $d = 2$ and $U(\mathbf{x}) = U_{\text{Lap}}(\mathbf{x})$ in (1.1)-(1.2). Again, the problem is solved numerically on a bounded computational domain $\Omega = [-16, 16]^2$ with time step $\tau = 10^{-4}$ and different mesh size h . Table 14 shows the errors of the wave-function and the 2D Coulomb interaction at $t = 0.5$ obtained by the TS-NUFFT method for different mesh size h and interaction constant β . We remark here that*

Table 13: Errors of the wave-function and the nonlocal interaction at $t = 1/8$ for the NLSE with the 3D Coulomb interaction.

TS-NUFFT	$h = 1$	$h = 1/2$	$h = 1/4$	$h = 1/8$	
$e_{\psi}^h(1/8)$	$\beta = -5$	5.461E-03	1.011E-05	9.297E-12	1.492E-13
	$\beta = 5$	3.997E-03	7.879E-06	6.959E-12	1.348E-13
$e_{\varphi}^h(1/8)$	$\beta = -5$	7.890E-03	4.466E-06	4.745E-12	6.992E-14
	$\beta = 5$	6.563E-03	2.828E-06	1.081E-12	6.872E-14
TS-DST	$h = 1$	$h = 1/2$	$h = 1/4$	$h = 1/8$	
$e_{\psi}^h(1/8)$	$\beta = -5$	2.561E-02	3.024E-02	3.025E-02	3.025E-02
	$\beta = 5$	2.753E-02	3.024E-02	3.025E-02	3.025E-02
$e_{\rho}^h(1/8)$	$\beta = -5$	5.567E-03	1.444E-05	2.397E-07	2.441E-07
	$\beta = 5$	5.590E-03	1.416E-05	2.560E-07	2.568E-07
$e_{\varphi}^h(1/8)$	$\beta = -5$	1.099E-01	1.099E-01	1.099E-01	1.099E-01
	$\beta = 5$	1.117E-01	1.117E-01	1.117E-01	1.117E-01

Table 14: Errors of the wave-function and the nonlocal interaction at $t = 0.5$ for the NLSE with the 2D Coulomb interaction.

TS-NUFFT ($L = 16$)	$h = 1$	$h = 1/2$	$h = 1/4$	$h = 1/8$	
$e_{\psi}^h(0.5)$	$\beta = -5$	1.582E-01	7.468E-03	4.746E-06	2.954E-12
	$\beta = 5$	5.118E-02	7.756E-04	2.476E-10	1.268E-12
$e_{\varphi}^h(0.5)$	$\beta = -5$	2.219E-02	4.242E-03	4.169E-06	3.756E-12
	$\beta = 5$	3.235E-02	2.451E-04	3.117E-11	7.586E-13
TS-DST ($L = 16$)	$h = 1$	$h = 1/2$	$h = 1/4$	$h = 1/8$	
$e_{\psi}^h(0.5)$	$\beta = -5$	1.175E-01	5.576E-02	6.311E-02	6.312E-02
	$\beta = 5$	6.477E-02	6.308E-02	6.313E-02	6.313E-02
$e_{\varphi}^h(0.5)$	$\beta = -5$	4.286E-02	2.449E-02	2.449E-02	2.449E-02
	$\beta = 5$	6.854E-02	4.412E-02	4.455E-02	4.478E-02
TS-DST ($h = 1/8$)	$L = 8$	$L = 16$	$L = 32$	$L = 64$	
$e_{\psi}^h(0.5)$	$\beta = -5$	1.263E-01	6.312E-02	3.156E-02	1.578E-02
	$\beta = 5$	1.264E-01	6.313E-02	3.156E-02	1.578E-02
$e_{\varphi}^h(0.5)$	$\beta = -5$	4.907E-02	2.449E-02	1.021E-02	4.999E-03
	$\beta = 5$	9.038E-02	4.500E-02	1.875E-02	9.181E-03

the *TS-DST* method is not applicable for this case [35, 41], therefore here we only present the results for the *TS-NUFFT* method.

Table 15: Errors of the wave-function and the Poisson potential at $t = 0.5$ for the NLSE with the 2D Poisson potential.

TS-NUFFT	$h = 1$	$h = 1/2$	$h = 1/4$	$h = 1/8$
$e_{\psi}^h(0.5)_{\beta = -5}$	5.833E-02	2.599E-04	3.211E-09	7.524E-13
$e_{\psi}^h(0.5)_{\beta = 5}$	2.658E-02	9.083E-05	3.395E-12	1.124E-12
$e_{\varphi}^h(0.5)_{\beta = -5}$	1.329E-02	8.840E-05	1.072E-09	3.974E-13
$e_{\varphi}^h(0.5)_{\beta = 5}$	4.645E-03	2.805E-06	8.322E-13	5.821E-13

From Tables 13–15 and additional numerical results not shown here for brevity, we can draw the following conclusions: (i) The *TS-DST*, if applicable, can not resolve the wave-function or the potential very accurately, while the *TS-NUFFT* achieves the spectral accuracy; (ii) The saturated accuracy by *TS-DST* decreases as the computation domain increases; (iii) As long as for the physical observables, e.g. the density ρ , are concerned, the *TS-DST* method can still capture reasonable accuracy (cf. Tab. 13).

4.3 Applications

To further demonstrate the efficiency and accuracy of the numerical method via the NUFFT, we simulate the long-time dynamics of the 2D NLSE with the Coulomb interaction, i.e. $d = 2$ and $U(\mathbf{x}) = U_{\text{Cou}}(\mathbf{x})$ and $\beta = 5$ in (1.1)-(1.2), and a honeycomb external potential [9, 20] defined as

$$V(\mathbf{x}) = 10 [\cos(\mathbf{b}_1 \cdot \mathbf{x}) + \cos(\mathbf{b}_2 \cdot \mathbf{x}) + \cos((\mathbf{b}_1 + \mathbf{b}_2) \cdot \mathbf{x})], \quad \mathbf{x} = (x, y)^T \in \mathbb{R}^2 \quad (4.6)$$

with $\mathbf{b}_1 = \frac{\pi}{4}(\sqrt{3}, 1)^T$ and $\mathbf{b}_2 = \frac{\pi}{4}(-\sqrt{3}, 1)^T$. This example can be formally used to describe the dynamics of the electrons in a graphene. The initial data in (1.3) is taken as $\psi_0(x, y) = e^{-(x^2+y^2)/2}$ for $\mathbf{x} \in \mathbb{R}^2$ and the problem is solved numerically on $\Omega = [-32, 32]^2$ by using the *TS-NUFFT* with mesh size $h = \frac{1}{16}$ and time step $\tau = 10^{-4}$. Figure 2 shows the contour plots of the density $\rho(x, y, t)$ at different times.

5 Conclusion

An efficient and accurate numerical method via the NUFFT was proposed for the fast evaluation of different nonlocal interactions including the Coulomb interactions in 3D/2D and the interaction kernel taken as either the Green's function of the Laplace operator in 3D/2D/1D or nonlocal interaction kernels in 2D/1D obtained from the 3D Schrödinger-Poisson system under strongly external confining potentials via dimension reduction. The method was compared extensively with those existing numerical methods and was demonstrated that it can achieve much more accurate numerical results, especially on a smaller bounded computational domain and/or with anisotropic interaction density. Then efficient and accurate numerical methods were presented for computing the ground state and dynamics of the nonlinear Schrödinger equation with nonlocal interactions by adapting the normalized gradient flow with the backward Euler Fourier pseudospectral discretization and time-splitting Fourier pseudospectral method, respectively, together with the fast and accurate NUFFT method for evaluating the nonlocal interactions. Extensive numerical comparisons were carried out between the proposed numerical methods and other existing methods in terms of ground state and dynamics of the NLSE with different nonlocal interactions. Numerical results showed that the methods via the NUFFT perform much better than those existing methods in terms of accuracy and/or efficiency as well as the nonlocal interaction potentials evaluation, especially when the bounded computational domain is chosen smaller and/or the solution is anisotropic.

Acknowledgments

Part of this work was done when the authors were visiting Beijing Computational Science Research Center in the summer of 2014. We acknowledge support from the Ministry of Education of Singapore grant R-146-000-196-112 (W. Bao), the National Science Foundation under grant CCF-0905395 (S. Jiang), the French ANR-12-MONU-0007-02 BECASIM (Q. Tang) and the Austrian Science Foundation (FWF) under grant No F41 (project VI-COM), grant No I830 (project LODIQUAS) and the Austrian Ministry of Science and Research via its grant for the WPI (Q. Tang and Y. Zhang). The computation results presented have been achieved by using the Vienna Scientific Cluster.

References

- [1] M. Abbamowitz and I. A. Stegun, Handbook of Mathematical Functions, Dover, 1965.
- [2] X. Antoine, W. Bao and C. Besse, Computational methods for the dynamics of the nonlinear Schrödinger/Gross-Pitaevskii equations, *Comput. Phys. Commun.* 184 (2013) 2621–2633.
- [3] X. Antoine, R. Duboscq, Robust and efficient preconditioned Krylov spectral solvers for computing the ground states of fast rotating and strongly interacting Bose-Einstein condensates, *J. Comput. Phys.* 258 (2014) 509–523.
- [4] W. Bao, N. Ben Abdallah and Y. Cai, Gross-Pitaevskii-Poisson equations for dipolar Bose-Einstein condensate with anisotropic confinement, *SIAM J. Math. Anal.* 44 (2012) 1713–1741.
- [5] W. Bao and Y. Cai, Mathematical theory and numerical methods for Bose-Einstein condensation, *Kinet. Relat. Mod.* 6 (2013) 1–135.
- [6] W. Bao, Y. Cai and H. Wang, Efficient numerical methods for computing ground states and dynamics of dipolar Bose-Einstein condensates, *J. Comput. Phys.* 229 (2010) 7874–7892.
- [7] W. Bao, I-L. Chern and F. Lim, Efficient and spectrally accurate numerical methods for computing ground and first excited states in Bose-Einstein condensates, *J. Comput. Phys.* 219 (2006) 836–854.
- [8] W. Bao and Q. Du, Computing the ground state solution of Bose-Einstein condensates by a normalized gradient flow, *SIAM J. Sci. Comput.* 25 (2004) 1674–1697.
- [9] W. Bao, H. Jian, N. J. Mauser and Y. Zhang, Dimension reduction of the Schrödinger equation with Coulomb and anisotropic confining potentials, *SIAM J. Appl. Math.* 73 (6) (2013) 2100–2123.
- [10] W. Bao, D. Marahrens, Q. Tang and Y. Zhang, A simple and efficient numerical method for computing the dynamics of rotating Bose-Einstein condensates via a rotating Lagrangian coordinate, *SIAM J. Sci. Comput.* 35 (6) (2013) A2671–A2695.

- [11] W. Bao, N. J. Mauser and H. P. Stimming, Effective one particle quantum dynamics of electrons: A numerical study of the Schrödinger-Poisson- $X\alpha$ model, *Comm. Math. Sci.* 1 (2003) 809–831.
- [12] C. Bardos, L. Erdős, F. Golse, N. J. Mauser and H.-T. Yau, Derivation of the Schrödinger-Poisson equation from the quantum N -particle Coulomb problem, *C. R. Math. Acad. Sci. Paris* 334(6) (2002) 515–520.
- [13] C. Bardos, F. Golse and N. J. Mauser, Weak coupling limit of the N -particle Schrödinger equation, *Methods Appl. Anal.* 7(2) (2000) 275–293.
- [14] C. Bardos and N. J. Mauser, The weak coupling limit for systems of N goes to infinity quantum particles. State of the art and applications, *J. Soc. Math. Française* (2003) 1–14.
- [15] N. Ben Abdallah, F. Méhats and O. Pinaud, Adiabatic approximation of the Schrödinger-Poisson system with a partial confinement, *SIAM J. Math. Anal.* 36 (2005) 986–1013.
- [16] O. Bokanowski, J. L. López and J. Soler, On a exchange interaction model for quantum transport: The Schrödinger-Poisson-Slater system, *Math. Model Methods Appl. Sci.* 12 (10) (2003) 1397–1412.
- [17] Y. Cai, M. Rosenkranz, Z. Lei and W. Bao, Mean-field regime of trapped dipolar Bose-Einstein condensates in one and two dimensions, *Phys. Rev. A* 82 (2010) 043623.
- [18] I. Catto, J. Dolbeault, O. Sánchez and J. Soler, Existence of steady states for the Maxwell-Schrödinger-Poisson system: exploring the applicability of the concentration-compactness principle, *Math. Model Methods Appl. Sci.* 23 (10) (2013) 1915–1938.
- [19] T. Cazenave, *Semilinear Schrödinger equations*, Courant Lecture Notes in Mathematics, vol. 10, New York University Courant Institute of Mathematical Sciences AMS, 2003.
- [20] Z. Chen and B. Wu, Bose-Einstein condensate in a honeycomb optical lattice: fingerprint of superfluidity at the Dirac point, *Phys. Rev. Lett.* 107 (2011) 065301.
- [21] X. Dong, A short note on simplified pseudospectral methods for computing ground state and dynamics of spherically symmetric

- Schrödinger-Poisson-Slater system, *J. Comput. Phys.* 230 (2011) 7917–7922.
- [22] A. Dutt and V. Rokhlin, Fast Fourier transforms for nonequispaced data, *SIAM J. Sci. Comput.* 14 (1993) 1368–1393.
- [23] L. Erdős and H.-T. Yau, Derivation of the nonlinear Schrödinger equation from a many body Coulomb system, *Adv. Theor. Math. Phys.* 5 (2001) 1169–1205.
- [24] F. Ethridge and L. Greengard, A new fast-multipole accelerated Poisson solver in two dimensions, *SIAM J. Sci. Comput.* 23 (3) (2001) 741–760.
- [25] Z. Gimbutas, L. Greengard and M. Minion, Coulomb interactions on planar structures: inverting the square root of the Laplacian, *SIAM J. Sci. Comput.* 22 (6) (2000) 2093–2108.
- [26] L. Greengard and J.Y. Lee, Accelerating the nonuniform fast Fourier transform, *SIAM Rev.* 46 (2004) 443–454.
- [27] L. Greengard and V. Rokhlin, A new version of the fast multipole method for the Laplace equation in three dimensions, *Acta Numerica* 6 (1997) 229–269.
- [28] H. Han and W. Bao, Error estimates for the finite element approximation of problems in unbounded domains, *SIAM J. Numer. Anal.* 37 (2000) 1101–1119.
- [29] S. Jiang, L. Greengard and W. Bao, Fast and Accurate Evaluation of Nonlocal Coulomb and Dipole-Dipole Interactions via the Nonuniform FFT, *SIAM J. Sci. Comput.* 36 (2014) B777–B794.
- [30] S. Jin, H. Wu and X. Yang, A numerical study of the Gaussian beam methods for one-dimensional Schrödinger-Poisson equations, *J. Comput. Math* 28 (2010) 261–272.
- [31] Ch. Lubich, On splitting methods for Schrödinger-Poisson and cubic nonlinear Schrödinger equations, *Math. Comp.* 77 (2008) 2141–2153.
- [32] P. A. Markowich, C. Ringhofer and C. Schmeiser, *Semiconductor Equations*, Springer-Verlag, 1990.
- [33] S. Masaki, Energy solution to a Schrödinger-Poisson system in the two-dimensional whole space, *SIAM J. Math. Anal.* 43 (2011) 2719–2731.

- [34] F. Méhats, Analysis of a quantum subband model for the transport of partially confined charged particles, *Monatsh. Math.* 147 (2006) 43–73.
- [35] N. J. Norbert and Y. Zhang, Exact artificial boundary condition for the Poisson equation in the simulation of the 2D Schrödinger-Poisson system, *Commun. Comput. Phys.* 16 (3) (2014) 764–780.
- [36] Ó. Sánchez and J. Soler, Long-Time Dynamics of the Schrödinger-Poisson-Slater Systems, *J. Statist. Phys.* 114 (2004) 179–204.
- [37] H.P. Stimming and Y. Zhang, A novel nonlocal potential solver based on nonuniform FFT for efficient simulation of the Davey-Stewartson equations, submitted.
- [38] G. Strang, On the construction and comparison of difference schemes, *SIAM J. Numer. Anal.* 5 (1968) 505–517.
- [39] M. Thalhammer, High-order exponential operator splitting methods for time-dependent Schrödinger equations, *SIAM J. Numer. Anal.* 46 (2008) 2022–2038.
- [40] H. Yoshida, Construction of higher order symplectic integrators, *Phys. Lett. A.* 150 (1990) 262–268.
- [41] Y. Zhang and X. Dong, On the computation of ground states and dynamics of Schrödinger-Poisson-Slater system, *J. Comput. Phys.* 230 (2011) 2660–2676.

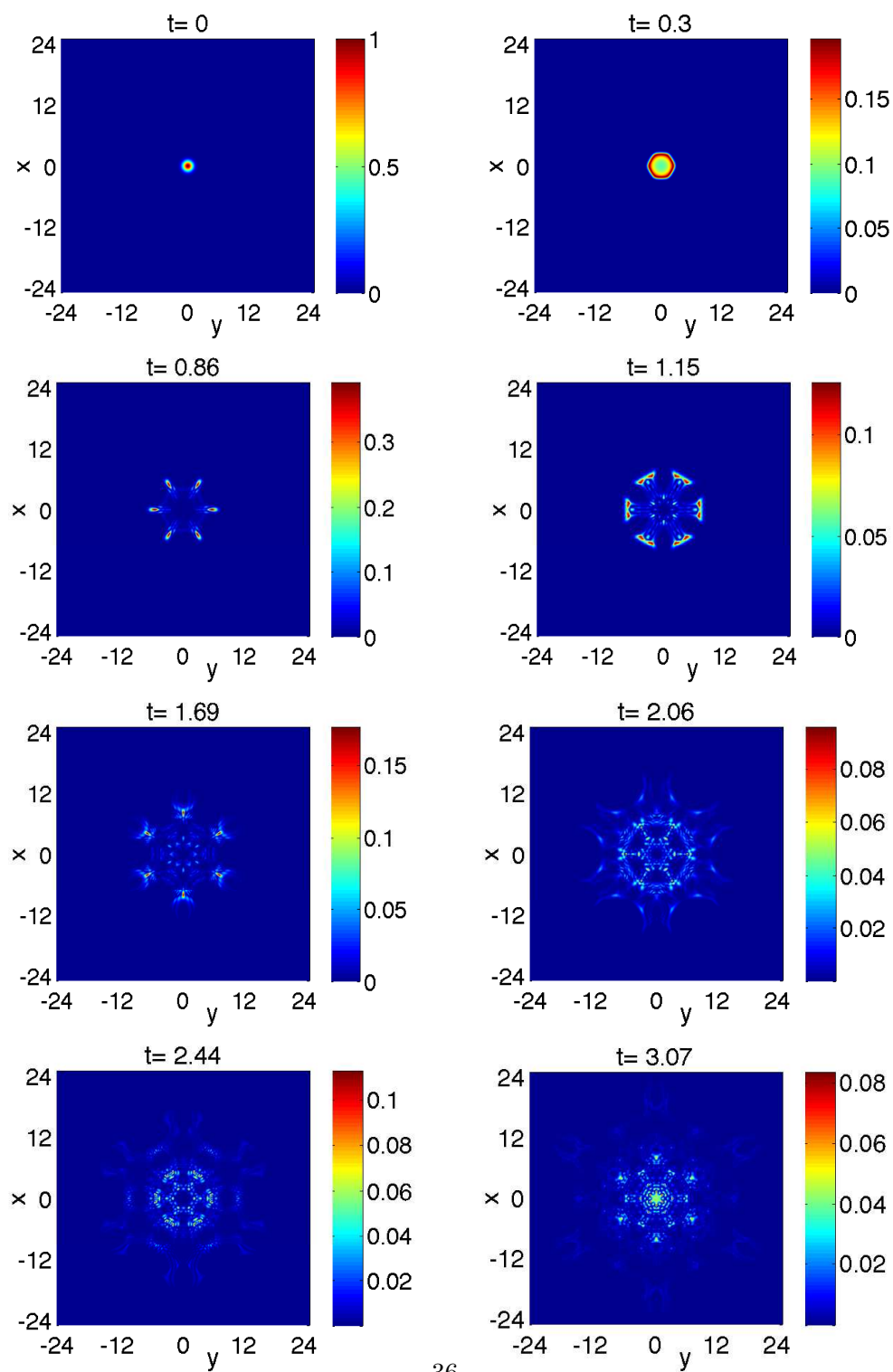


Figure 2: Contour plots of the density $\rho(x, y, t)$ of the NLSE with the Coulomb interaction and a honeycomb potential in 2D at different times.